



Chemical and thermal analysis of troctolite, Hamragarðaheiði, Eyjafjöll, Iceland

Viktor Þór Georgsson



**Faculty of Earth Science
University of Iceland
2016**

Chemical and thermal analysis of troctolite, Hamragarðaheiði, Eyjafjöll, Iceland

Viktor Þór Georgsson

10ECTS thesis submitted in partial fulfilment of
Baccalaureus Scientiarum degree in Geology

Advisor
Enikő Bali

Faculty of Earth Science
School of Engineering and Natural Sciences
University of Iceland
Reykjavík, June 2016

Chemical and thermal analyses of troctolite, Hamragarðaheiði, Eyjafjöll, Iceland
Chemical and thermal analyses of troctolite
10ECTS thesis submitted in partial fulfilment of *Baccalaureus Scientiarum* degree in
Geology

Copyright © 2016 Viktor Þór Georgsson
All rights reserved

Faculty of Earth Science
School of Engineering and Natural Sciences
University of Iceland
Askja, Sturlugata 7
101 Reykjavík

Telephone: 525 4000

Registration information:
Viktor Þór Georgsson, 2016, *Chemical and thermal analysis of troctolite, Hamragarðaheiði, Eyjafjöll, Iceland*, BS thesis, Faculty of Earth science, University of Iceland, 58 pages.

Printing: Háskólaprent
Reykjavík, May 2016

Abstract

This study describes the minerals in a troctolite xenolith from Hamragarðaheiði, Iceland, and its melt inclusions. Studies of xenoliths from deep inside the crust provide an interesting picture on crustal structure and on the mantle-crust interaction (Gurenko & Sobolev, 2006). Previous studies and available literature on Icelandic crustal xenoliths are rare, this thesis provides additional knowledge to that list and furthers the understanding on mantle-crust relations beneath Iceland.

Olivine in the troctolite have $\text{Fo}_{61.6-78.2}$ showing high MgO concentration of 30.45-41.32 wt%, and FeO ranging from 20.16-33.83 wt%. Plagioclase are mostly labradorite and bytownite with $\text{An}_{41.75-87.37}$. Al_2O_3 was measured in the range of 26.64-36.15 wt.% and CaO had a wide range of 9.39-18.77 wt.%. The pyroxene has high MgO concentration in the range of 13.83-16.97 wt.% giving them a Mg# in the range of 74.3-80.2. Compositions in the pyroxene are $\text{Wo}_{39.77-45.89}\text{En}_{40.98-48.39}\text{Fs}_{11.48-14.55}$, which makes them cluster at the border between augite and diopside. The melt inclusions, corrected for post entrapment modification, have a Mg# ranging from 33.86-51.69, they have Al_2O_3 concentration in the range of 11.36-18.75 wt.%, the FeO concentration ranges from 5.54-18.29 wt.%, MgO has the range of 3.03-8.95 wt.%, and CaO concentration ranges from 10.04-15.21. Comparison between the chemical compositions in the troctolite to chemical compositions in the host rock and from the eruption at Fimmvörðuháls 2010 show much similarities.

Thermal calculations were carried out on olivine hosted and plagioclase hosted melt inclusions in the troctolite and they show an average temperature of crystallization at $1147 \pm 45^\circ\text{C}$.

Útdráttur

Rannsóknin sem hér verður fjallað um lýsir steindum og glerinnlyksum úr troktólít framandstein sem fannst á Hamragarðsheiði, Íslandi. Rannsóknir á framandsteinum sem eru frá miklu dýpi í skorpunni geta veitt áhugaverða mynd af byggingu skorpunnar og samskiptum möttuls við skorpuna (Gurenko & Sobolev, 2006). Fyrri rannsóknir og aðgengileg rit um framandsteina á Íslandi eru sjaldgæf, þessi ritgerð bætir við þekkingu á þessu sviði og hjálpar til við að efla skilning á samskiptum möttuls og skorpu undir Íslandi.

Ólivín steindir í troktólítinu hafa $\text{Fo}_{61,6-78,2}$ sem samsvarar háu þyngdarhlutfalli MgO sem er á bilinu 30,45-41,32 % og styrk FeO á bilinu 20,16-33,83 %. Plagíóklas steindirnar eru aðalega af gerðinni labradorít og bytownít og hafa $\text{An}_{41,75-87,37}$. Þyngdarhlutfall Al_2O_3 var mælt á bilinu 26,64-36,15 % og styrkur CaO var frekar fjölbreyttur og mældist á bilinu 9,39-18,77 %. Pýroxen steindirnar mældust með hátt MgO þyngdarhlutfall á bilinu 13,83-16,97 %, sem sést í hárri Mg\# steindanna sem er á bilinu 74,3-80,2. Kristöllun pýroxen steindanna er frekar einsleit ($\text{Wo}_{39,77-45,89}\text{En}_{40,98-48,39}\text{Fs}_{11,48-14,55}$), sem setur gerð steindanna við mörkin á milli augít og díopsíd. Efnasamsetning glerinnlyksanna, leiðrétt fyrir breytingar sem þær verða fyrir eftir að hafa innlokast, sýnir Mg\# á bilinu 33,86-51,69, þyngdarhlutfall Al_2O_3 mældist 11,36-18,75 %, styrkur FeO var á bilinu 5,54-18,29 %, MgO mældist 3,03-8,95 % og þyngdarhlutfall CaO var á bilinu 10,04-15,21 %. Þegar efnasamsetning glerinnlyksanna var borin saman við efnasamsetningar í hrauninu utan um framandsteininn og einnig við glerinnlyksur frá Fimmvörðuháls gosinu 2010, þá sést að samsvörun er á milli þessara efnasamsetninga.

Hitastig kristöllumunar var reiknað hjá glerinnlyksunum, bæði hjá þeim sem fundust í plagíóklas og ólivín, útreikningar sýndu að meðalhitastig allra glerinnlyksanna er $1147 \pm 45^\circ\text{C}$.

Table of Contents

List of figures	vii
List of tables	ix
Abbreviations.....	x
Acknowledgements	xi
1 Introduction.....	1
1.1 Troctolite	2
1.2 Olivine.....	2
1.3 Plagioclase.....	3
1.4 Pyroxene.....	4
2 Geological setting	5
3 Method	7
3.1 Thin section	7
3.2 Scanning electron microscope (SEM).....	7
3.3 Thermobarometric calculation	9
3.3.1 “Glass” (or liquid) thermometers.....	9
3.3.2 Olivine-liquid thermometer	10
3.3.3 Plagioclase- and alkali feldspar-liquid thermobarometers.....	10
3.4 Re-equilibration of melt inclusions	11
4 Results	13
4.1 Petrography	13
4.2 Chemical analyses	14
4.2.1 Olivine.....	14
4.2.2 Plagioclase	16
4.2.3 Pyroxene	19
4.2.4 Melt inclusions.....	23
4.3 Thermal calculations for melt inclusions	27
5 Discussion	29
5.1 Chemical analyses	29
5.2 Thermal calculation.....	29
6 Summary and Conclusions	31
References.....	33
Appendix A.....	37
Appendix B.....	39

Appendix C	41
Appendix D	43

List of figures

Figure 1: Diagram of olivine-bearing gabbroic rocks (Sandatlas, 2016).	2
Figure 2: Ternary diagram for feldspars (Carleton, 2015).	3
Figure 3: Ternary diagram for pyroxene (Morimoto, 1988)	4
Figure 4: Map of the south coast of Iceland, showing volcanos, rivers, and glaciers. The upper left corner shows a map of Iceland where the volcanic zones are shown (Jakobsson, 1979).....	5
Figure 5: Diagram of SEM showing the main components (Purdue University, 2014)	8
Figure 6: example of chemical analyses in the SEM.	9
Figure 7: Schematic representation of post entrapment crystallization (PEC). The melt inclusion crystallizes along the interface with the crystal and decreases in volume. This process can create a shrinkage bubble (UO BLOGS, 2016).....	11
Figure 8: Images from the microscope (left, crossed polarized light) and SEM (right) of the minerals and melt inclusions in the troctolite. Note, the high interference colours of plagioclase is due to a larger than 30 μm thickness of the thin section.....	13
Figure 9: BSE image of olivine showing a darker core with lighter rims. Note the oxide inclusion in the core.	14
Figure 10: Comparison of olivine in the troctolite and olivine from the host rock. Comparative data from Kristjánssin (2015) and Enikö Bali. The histogram shows nr. of olivine as a function of Fo contents.	16
Figure 11: Ternary diagram showing plagioclase compositions in the troctolite and host rock. Comparative data are from Helgadóttir (2016).....	17
Figure 12: Comparison of plagioclase in the troctolite and plagioclase from the host rock. Comparative data from Helgadóttir (2016). The graph shows nr. of plagioclase as a function of An content.	19
Figure 13: Ternary diagram showing pyroxene compositions in the troctolite. The black circle represents pyroxenes from the host rock analysed by Gísladóttir (2015).....	20
Figure 14: Comparison of pyroxene in the troctolite and pyroxene from the host rock. Comparative data from Gísladóttir (2015). The graph shows nr. of pyroxene as a function of Mg#.	22

Figure 15: Comparison of pyroxene in the troctolite and pyroxene from the host rock. Comparative data from Gísladóttir (2015). The graph shows nr. of pyroxene as a function of Mg#.....	22
Figure 16: TAS diagram for melt inclusions before (triangles) and after (dots) post entrapment correction. mi. stands for melt inclusions.....	24
Figure 17: Comparison of the wt.% for SiO ₂ , FeO, and Al ₂ O ₃ as a function of Mg# in the melt inclusions.....	26
Figure 18: Graph showing thermal calculations in olivine and plagioclase hosted melt inclusions with the SEE for each equation.	28
Figure 19: A screenshot of equation (13) from Putirka (2008).....	37
Figure 20: A screenshot of equations (14) and (15) from Putirka (2008).....	37
Figure 21: A screenshot of equation (16) from Putirka (2008).....	37
Figure 22: A screenshot of equation (19) from Putirka (2008).....	37
Figure 23: A screenshot of equation (20) from Putirka (2008).....	37
Figure 24: A screenshot of equations (21) and (22) from Putirka (2008).....	38
Figure 25: A screenshot of equation (23) from Putirka (2008).....	38
Figure 26: A screenshot of equations (24a) and (26) from Putirka (2008).....	38
Figure 27: Graph showing the trend of re-equilibration from 0-25%, with melt inclusions compositions from Moune et al. (2012) and groundmass in host rock from Kristjánsson (2015).....	41
Figure 28: Pictures from the polarization microscope of olivine, plagioclase and melt inclusions. A shows olivine with several melt inclusions. B is a melt inclusion in reflective light. C a zoned plagioclase with many melt inclusions in the core. D close-up of a melt inclusion in the plagioclase from C by reflected light. E a zoned olivine at the contact with the host rock. F zoned plagioclase.	43
Figure 29: SEM pictures of the troctolite. A shows two melt inclusion in olivine along with spinel. B and C chemical maps of a melt inclusion and a spinel from A. D shows three melt inclusions in plagioclase. E showing olivine, oxide, pyroxene and melt inclusions, note the dark haloes around them indicating extensive PEC. F chemical map of the same area as in E, here one can observe a rather large phosphorus rich crack in the bottom of the photo.....	44

List of tables

Table 1: Chemical composition of olivines.....	15
Table 2: Chemical compositions of plagioclases.	18
Table 3: Chemical compositions of pyroxenes.	21
Table 4: Re-equilibrated compositions of melt inclusions. Blue samples are plagioclase hosted and green samples are olivine hosted.....	25
Table 5: Results for the thermal calculations in olivine hosted melt inclusions. Showing for fixed pressure of 0.5 GPa. K_D is green if chemical equilibrium can be assumed (it falls into the range of 0.3 ± 0.03).	27
Table 6: Results for the thermal calculations on plagioclase hosted melt inclusions. Showing for fixed pressure of 0.5 GPa. K_D is green if chemical equilibrium can be assumed (it falls into the range of 0.27 ± 0.11).	28
Table 7: Raw chemical analyses of melt inclusions. Blue samples are plagioclase hosted and green samples are olivine hosted.....	39

Abbreviations

Fo – Forsterite

Fa – Fayalite

Ab – Albite

An – Anorthite

Or – Orthoclase

Wo – Wollastonite

En – Enstatite

Fs – Ferrosilite

EVZ – Eastern Volcanic Zone

SISZ – South Iceland Seismic Zone

m.a.s.l. – Meters above sea level

SEM – Scanning Electron Microscope

EDS – Energy Dispersive Spectrometer

PEC – Post Entrapment Crystallization

SEE – Standard Error of Estimate

Mg# – Magnesium number

P – Pressure

T – Temperature

GPa – Gigapascal

°C – Degrees Celsius

TAS – Total Alkali-Silica diagram

QFM – Quarts-Fayalite-Magnetite oxidation state

Acknowledgements

I would like to thank my supervisor Enikő Bali for her guidance during the work on this thesis, both on the lab work and in the writing. I would also like to thank Bryndís Ýr Gísladóttir, Kjartan Björgvin Kristjánsson and Þrúður Helgadóttir for providing me with the data on the host rock.

1 Introduction

This study describes a troctolite xenolith and its melt inclusions from Hamragarðaheiði, Eyjafjöll, Iceland. Previous studies and available literature on Icelandic crustal xenoliths seem to be in short supply with only one paper regarding gabbro xenoliths from Miðfell by Gurenko & Sobolev (2006), a MS thesis by Einarsson (2012). Troctolites, although they are not rare, are even more scarcely studied in Iceland. In the literature there is an abstract about troctolite/gabbro xenoliths from the Reykjanes peninsula by Grandvuinet et al. (2006), and a BSc thesis from the University of Gothenburg by Reyier (2013). Studies of xenoliths from deep inside the crust provide an interesting picture of the mantle-crust interaction. Gurenko & Sobolev (2006) say that “interaction of rising magma with crustal rocks or contaminations of primitive, mantle-derived magmas could be more common in Iceland compared to mid- ocean ridge basalt” (Gurenko & Sobolev, 2006).

This project was therefore very interesting, especially because the area where the troctolite block of this work was found is well studied. This makes it possible to compare the compositions of mineral constituents and melt inclusions to those in various lava compositions from the area. The purpose of this thesis was to chemically analyse the minerals and melt inclusions in the troctolite, and by utilizing thermometers from Putirka (2008) try to determine the temperature of crystallization. Also to compare these results to other works of similar nature.

1.1 Troctolite

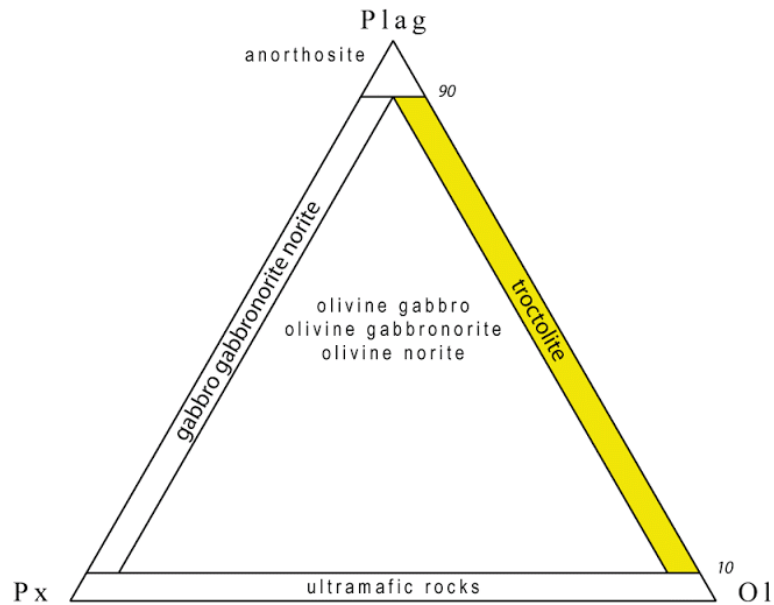


Figure 1: Diagram of olivine-bearing gabbroic rocks (Sandatlas, 2016).

Gabbros are an intrusive rock of basaltic composition with grains ranging in size from medium- to coarse-grained. There is a great variety in the modal and chemical composition of gabbroic rocks where some grade into the pyroxenites and peridotites, and others grade into the anorthosites. They resemble basalts in that their compositions which range from alkalic to tholeiitic types and they also include high Al_2O_3 and high MgO varieties. Troctolites are gabbroic rocks that are mostly composed of calcic plagioclase and olivine, with little or no pyroxene (Middlemost, 1985). Troctolite in general is constructed of olivine (45-64%, 1-4 mm), plagioclase (27-40%, 2-4 mm), clinopyroxene (2-15%, <1 mm) and spinel (0.5%, 0.5 mm). It has a mesocumulate texture where the cumulus phases are olivine and plagioclase and the intercumulus phase is clinopyroxene. Textural relationship shows that olivine and plagioclase start to precipitate together with the crystallization of olivine starting slightly earlier. The crystallization order of troctolite is inferred to be: $\text{Sp} + \text{Ol} - \text{Sp} + \text{Ol} + \text{Pl} - \text{Sp} + \text{Ol} + \text{Pl} - \text{Cpx}$ (Drouin, 2009). Renna & Tribuzio (2011) have shown that troctolite forms at the contact of a gabbroic pluton that has intruded into residual mantle peridotites.

1.2 Olivine

Olivine crystallizes with orthorhombic symmetry and the structure consists of independent SiO_4 tetrahedra that are linked by divalent cations in six-fold coordination. The structure itself is based on sheets of oxygen atoms parallel to (100) in a seemingly hexagonal-close-packed arrangement. Between the oxygen sheets there are sites of two types making the atoms there to be either octahedral or tetrahedral coordination. The general chemical formula for olivine is $(\text{Mg,Fe})_2\text{SiO}_4$ where the amount of Mg and Fe divides olivine into forsterite (Fo) (Mg_2SiO_4) and fayalite (Fa) (Fe_2SiO_4). Olivine is a major component of ultrabasic plutonic rocks and when they are of metamorphic origin it is mostly in rocks of ultramafic composition. Mg-rich olivine crystallizes first from a liquid as it cools, making

the residual liquid having higher Fe concentration. Some of the characteristics of olivines are its high relief, high birefringence in a polarization microscope and absence of a well-developed cleavage (Deer et al, 2013).

1.3 Plagioclase

Plagioclase is the most common rock-forming mineral in the Earth's crust. Its high temperature form is found in many volcanic igneous rocks while its low temperature form can be found in plutonic igneous rocks and metamorphic rocks. The chemical formula for the plagioclase series is $\text{NaAlSi}_3\text{O}_8$ (albite) – $\text{CaAl}_2\text{Si}_2\text{O}_8$ (anorthite). Plagioclase like alkali feldspar is a ternary solid solution of three components that are albite (Ab), anorthite (An) and orthoclase (Or), where the last one is usually in low concentration for plagioclase. Classification diagram for feldspars is shown in figure 2.

Plutonic plagioclase are almost all complex intergrowths at sub-optical scale. Solid solutions of plagioclase are subdivided purely on the basis of composition, $(\text{Ab} + \text{Or})_x\text{An}_{100-x}$: An 0-10: albite, 10-30: oligoclase, 30-50: andesine, 50-70: labradorite, 70-90: bytownite, 90-100: anorthite. Continuous variation in optical and physical properties of the plagioclase can be observed within different Ab:An ratios which may be used to determine composition (Deer et al, 2013).

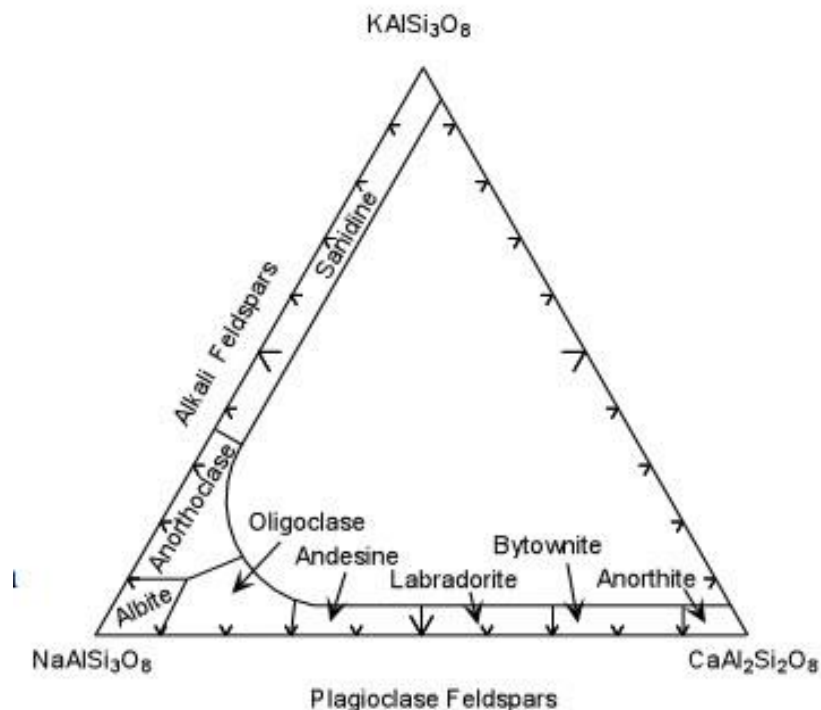


Figure 2: Ternary diagram for feldspars (Carleton, 2015).

1.4 Pyroxene

One of the most important group of rock-forming ferromagnesian silicates are the pyroxenes. They can be found in widely different rock compositions that is formed during regional and contact metamorphism or igneous processes. Pyroxenes can be either orthorhombic or monoclinic where the first has a simple chemical series, $(\text{Mg,Fe})\text{SiO}_3$, and the latter is a larger group with a very wide range of chemical composition. In broad terms there are three major subgroups for pyroxenes and they are magnesium-iron pyroxenes, calcium-rich pyroxenes and sodium-rich pyroxenes (Morimoto, 1988). Ternary diagram for pyroxene is shown in figure 3, the different type of minerals that are considered to be pyroxene are also marked on it. CaSiO_3 is the chemical formula for wollastonite (Wo) and is on top of the diagram for pyroxene but does not have a pyroxene structure, it is considered a pyroxenoid (Tulane University, 2011). MgSiO_3 is enstatite (En) and FeSiO_3 is ferrosilite (Fs). The most common Ca-rich pyroxenes in igneous rocks have diopside or augite compositions. The formula for pyroxenes can be expressed in structural terms as $\text{M}_2\text{M}_1\text{T}_2\text{O}_6$, where M2 and M1 are cations in generally distorted and regular octahedral coordination, respectively, and T is for tetrahedrally coordinated cations (Deer et al, 2013).

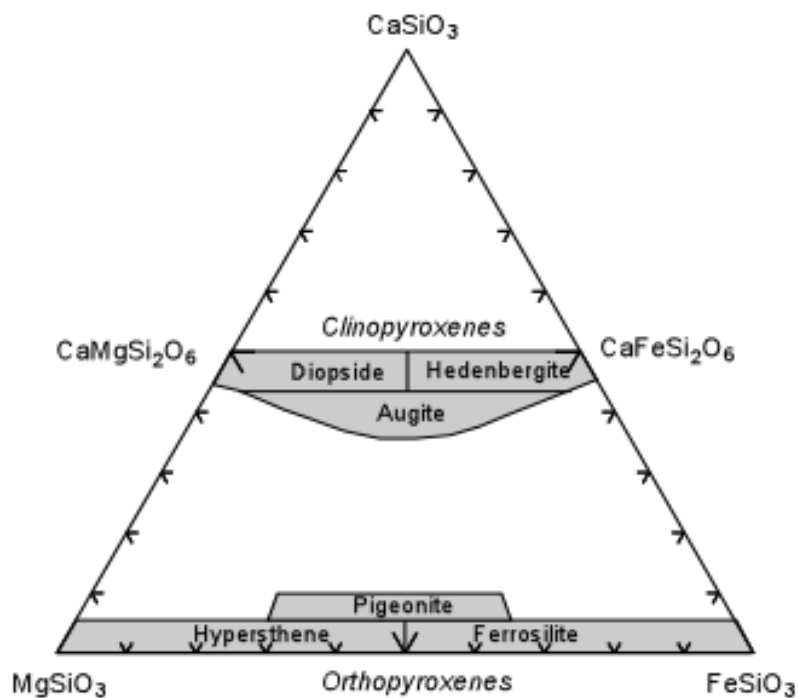


Figure 3: Ternary diagram for pyroxene (Morimoto, 1988)

2 Geological setting

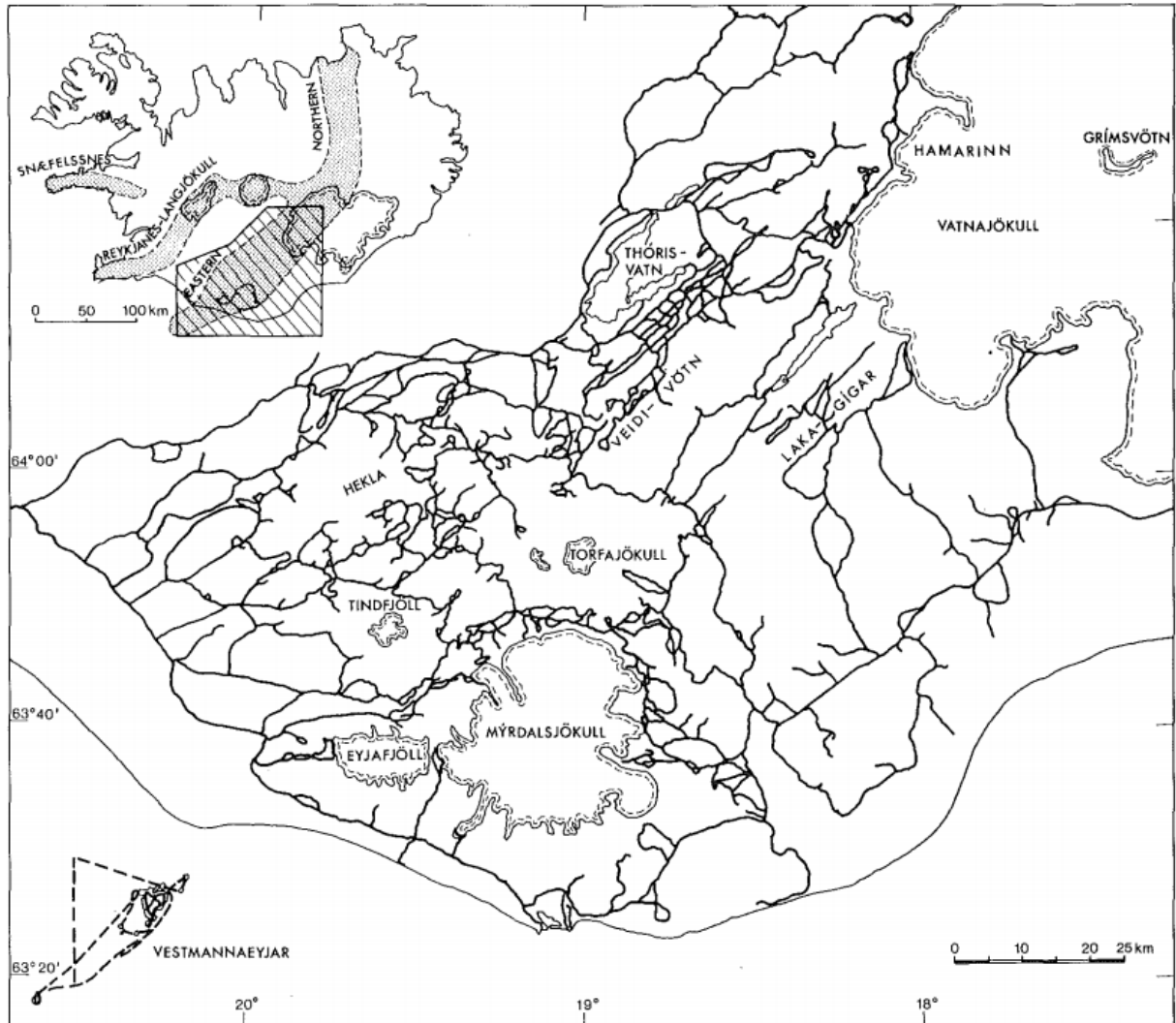


Figure 4: Map of the south coast of Iceland, showing volcanos, rivers, and glaciers. The upper left corner shows a map of Iceland where the volcanic zones are shown (Jakobsson, 1979).

One of the most active volcanic areas on earth is Iceland, it averages 28-30 volcanic eruptions per century. Iceland is 85-90% igneous rock while 0.5% is considered to be intrusive or plutonic rock brought forth by shallow erosion, and 10-15% are consolidated sediments. Geological formations in Iceland are divided into four formations, Holocene (<0.01 Ma), Late-Pleistocene (0.01-0.78 Ma), Pliocene-Pleistocene (0.78-3.3 Ma) and Tertiary (3.3-16 Ma) (Sæmundsson, 1980). The Mid-Atlantic Ridge cuts Iceland from southwest to northeast of the island with a complex series of rift- and transform zones, and in the middle of it lies a hotspot that increases volcanic activity immensely. There are nine sections of Icelandic volcanic zones, Northern Reykjanes Ridge (NRR), Western Volcanic Zone (WVZ), Hofsjökull Volcanic Zone (HVZ), Eastern Volcanic Zone (EVZ), Northern Volcanic Zone (NVZ), Tjörnes Volcanic Zone (TVZ), Snæfellsnes Volcanic Zone (SVZ),

Öræfajökull Volcanic Zone (OVZ) and the South Iceland Seismic Zone (SISZ). The main rifting zones are NRR, WVZ, HVZ, EVZ and NVZ. Eruptions in the Late Pleistocene have been found in the SISZ but no volcanic systems seem to have arisen there. Research on 1378 major element chemical analyses from 41 volcanic systems, show that three volcanic rock series are found in Iceland, a tholeiitic, an alkalic and a transitional alkalic series. The Eyjafjöll area, along with other volcanos in southern Iceland, is classified as a transitional alkalic system. Basalts in the transitional rock series have high Fe and Ti content, and produce transitional olivine basalt and transitional basalt. Macrophenocrysts are usually poor in these types of rock but that is not true for the Eyjafjöll area. Silicic rocks of the transitional alkalic series are transitional rhyolites and transitional trachytes (Jakobsson et al., 2008).

Lying on the south coast of Iceland is the Eyjafjöll volcanic system, it starts immediately to the south of the Tindfjöll complex and borders on the west flank of the Katla volcanic system (Mýrdalsjökull). Located south of the rift-transform intersection where the EVZ and SISZ meet, the Eyjafjallajökull volcano rises 1668 m.a.s.l. and has a 2.5 km wide caldera (Jakopsson, 1979). The volcano is classed as a stratovolcano that is covered in an ice sheet and shows a more dormant behaviour than other Icelandic volcanos in the neovolcanic zone. Though Eyjafjallajökull is classified as a stratovolcano it is argued by Thordarson & Larsen (2007) that it does not fit the criteria and classification for a stratovolcano. It does on the other hand show close structural resemblance to polygenetic Hawaiian shields. Eruptive history shows that in recent time the volcano erupted in 1821 and 1823 with possible eruptions in 1612 and 920. Due to increasing seismicity and inflation in 1994 and 1999, monitoring was increased in light of possible volcanic unrest (Keiding & Sigmarsson, 2012).

Centuries of volcanism have built up the mountains of Eyjafjöll as Leó Kristjánsson's (1988) research shows. He says that volcanism in this region was happening at least 0.7 million years ago. It is customary to consider, in a whole, Eyjafjöll as a Hyaloclastite formation but it is generally recognized that the formation is in reality more complex than that. Jónsson (1998) argues that ankaramite is the most characteristic type of rock found in Eyjafjöll (Jónsson, 1998). Several lavas from the late Pleistocene have been identified and one of them is from Hvammsmúli which is close to Hamragarðaheiði where the troctolite block was found (Jakopsson, 1974). 20 small lavas from the early Holocene epoch have also been identified (Larsen et al., 2012).

The most recent eruption in the area happened in 2010. On the 20th of March 2010 a 300 m long fissure opened up on the western flanks of Fimmvörðuháls pass between Eyjafjallajökull and Mýrdalsjökull. Another fissure opened up on the 31st of March and soon after it became the main eruption vent. After 23 days the flank eruption ended after producing 0.025 km³ of eruptive material which was analysed as mildly alkali olivine- and plagioclase-phyric basalt (Moune et al, 2012). Two days later another eruption started west of Fimmvörðuháls in the summit of Eyjafjallajökull. That eruption was phreatomagmatic due to its subglacial location but after less than a week it had turned into a purely magmatic eruption, that eruption continued until the 22nd of May when it ended (Keiding & Sigmarsson, 2012).

3 Method

3.1 Thin section

One of the most used method to study minerals and rocks is the petrographic microscope. It uses polarized light to do measurements and rapid identification of unknown minerals in thin sections or grain mounts. Thin sections are prepared by cementing the desirable rock to a microscope slide and then grinding it down, usually to a thickness of 0.03 mm. Porous and friable samples need to be glued to the thin section with an epoxy that is forced into pores with a vacuum chamber. The final touch is either to cover the thin section with a coverslip or polishing the surface to a mirror like surface. Polarized light is produced in petrographic microscopes by placing a polarizing film in the optical path. The polarizing film has a sheet of plastic that is optically anisotropic and it splits unpolarized light into two plane-polarized rays that are at right angles to each other. In this process one ray is eliminated and the other one passes through as plane polarized light (Nesse, 2012).

The thin sections for this project had already been prepared and were ready for inspection. In total there were three thin sections from different parts of the troctolite. One from the contact with the host rock and two nearer to the core. All the thin sections were made a little thicker than normal so different types of analytical methods can be used on the same thin section. Main reason for the petrographic microscope analysis was to get familiar to the samples and mapping them before the SEM analyses.

3.2 Scanning electron microscope (SEM)

Scanning electron microscope or SEM is an instrument that can be used to observe minerals in high resolution and if equipped with Energy Dispersive Spectrometer (EDS), one can also determine the chemical composition of minerals. It functions like an electron microprobe except the detectors are different. While the microprobe detector detects X-rays the SEM detector records electrons that are emitted from the sample. SEM devices consist of a cathode ray tube that is evacuated of all air after the sample has been inserted, a tungsten filament that is heated so much it emits electrons, an anode plate which accelerates the electrons with a voltage of several tens of kilovolts through a hole provided in the anode plate, and a lens that focuses the electrons into a fine beam using electromagnetic fields from an electrical coil. Figure 5 shows schematically these main components. The sample is coated with carbon or gold so the electrons from the electron beam are conducted away. When the electron beam strikes a sample, electrons of two types are emitted from the surface. These electrons differ in magnitude of energy, the higher energy electrons are called backscatter electrons, while the lower energy electrons are called secondary electrons. The backscatter electrons are deflections from the electron beam when it interacts with the sample and secondary electrons are in turn dislodged from atoms in the sample. When an electron strikes the detector it produces a spark of light. From this light an electrical pulse is produced and the instrument records it as a count. The backscatter electrons are normally used to map compositions because elements of higher atomic weight scatter a higher fraction of the electron beam back out of the sample (Nesse,

2012). The back scatter signals are attained mainly from the topmost nanometers in the sample and therefore does not suffer much blurring of chemical contrast due to vertical chemical heterogeneity. Beam diameter controls the lateral resolution (Blundi & Cashman, 2008). Secondary electrons are used to generate images of shapes and topography. SEM images are produced by systematically sweeping the electron beam back and forth over the sample. Output is recorded by the detector for each pixel and is then plotted on a computer monitor by an electronics package (Nesse, 2012).

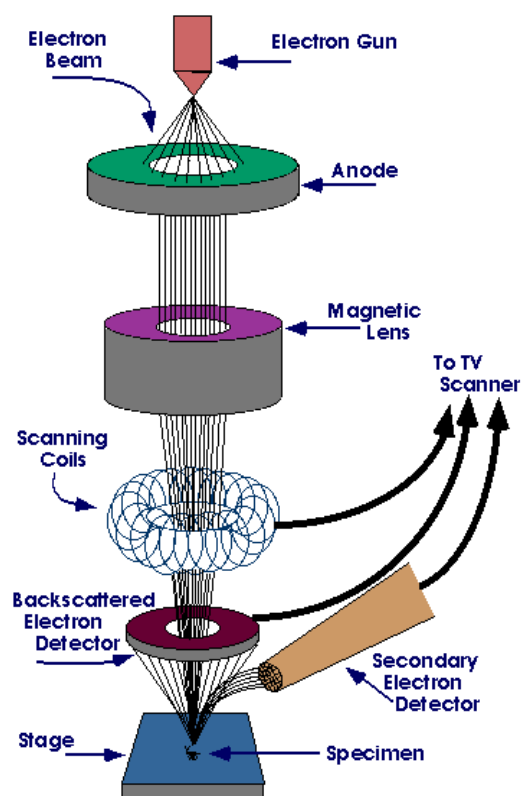


Figure 5: Diagram of SEM showing the main components (Purdue University, 2014)

For this project a Hitachi: TM3000 Tabletop SEM was used. The machine has an acceleration voltage of 5 kV or 15 kV with a tungsten source, a magnification of up to 30000x, and 30 nm resolution. The samples were coated with carbon to conduct the electrons. Measurements are carried out by selecting a point or marking an area on the mineral in question, picture of this can be seen in figure 6.

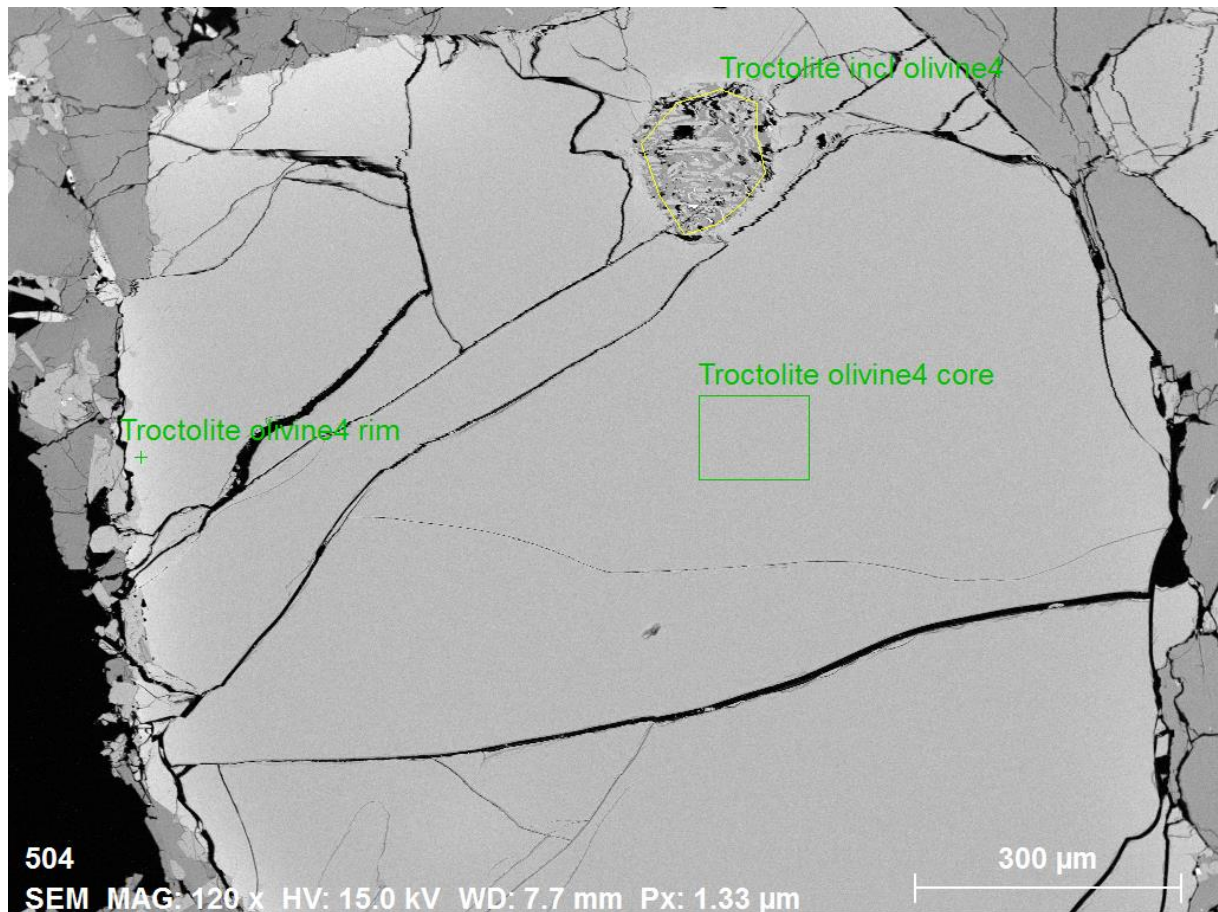


Figure 6: example of chemical analyses in the SEM.

The SEM-EDS measures chemicals in the selected area. These components are recalculated with the help of an EDS calibration Excel sheet, developed by Niels Oskarsson and Enikő Bali in order to obtain the chemical composition of the minerals. This Excel sheet contains mineral specific calibrations. It bases on multiple analyses of synthetic and natural standards.

3.3 Thermobarometric calculation

3.3.1 "Glass" (or liquid) thermometers

All equations for this section can be found in appendix A. Temperature of silicate melt can be calculated based on its major element composition. Although the calibration of Helz and Thornber (1987) and Montierth et al. (1995) thermometers are simple, they work well. Based on their calibration, melt temperature depends on wt% of MgO in a liquid. Putirka (2008) have updated their model to wipe out earlier systematic error and developed equation (13). This equation yields a standard error of estimate (SEE) of ± 71 °C. By adding additional compositional terms, error is reduced even further and it gives two more equations, one P-independent (14) and the other P-dependent (15). In these equations $Mg^{\#liq}$ is in molar ratios, other terms are weight percent oxides in a liquid or glass. Equation (14) has $SEE = \pm 51$ °C and equation (15) has $SEE = \pm 60$ °C. Equations (13)-(15) are appropriate for volcanic rocks that are saturated with olivine and other mineral phases, in the following P-T and compositional ranges: $P = 0.0001-14.4$ GPa; $T = 729-2000$ °C;

$\text{SiO}_2 = 31.5\text{-}73.64$ wt%; $\text{Na}_2\text{O}+\text{K}_2\text{O} = 0\text{-}14.3$ wt%; $\text{H}_2\text{O} = 0\text{-}18.6$ wt%. Improvements to this geothermometer were made by Yang et al. (1996) requiring additional phases to be in equilibrium with the liquid. It applies to liquids in equilibrium with olivine + plagioclase + clinopyroxene and gives equation (16). $X_{\text{MgO}}^{\text{liq}}$ is the mole fraction of MgO in the liquid. For equation (16) the two SEE calculated, $\text{SEE} = \pm 19$ °C and $\text{SEE} = \pm 26$ °C. Equation (16) does not work as well for liquids that are additionally saturated with other phases like spinel or other oxides (Putirka, 2008).

3.3.2 Olivine-liquid thermometer

Thermometers and barometers based on more than one phases need to have the phases in equilibrium, otherwise calculated P-T conditions have no meaning or at least very high uncertainties. Chemical equilibrium can be checked with the help of well known equilibrium constants. E.g.: Fe-Mg partitioning between olivine and liquid can be described by the reaction, $\text{MgO}^{\text{ol}} + \text{FeO}^{\text{liq}} \leftrightarrow \text{MgO}^{\text{liq}} + \text{FeO}^{\text{ol}}$. This shows that the equilibrium constant known as Fe-Mg exchange coefficient, or $K_D(\text{Fe-Mg})^{\text{ol-liq}} = [(X_{\text{Fe}}^{\text{ol}}X_{\text{Mg}}^{\text{liq}})/(X_{\text{Mg}}^{\text{ol}}X_{\text{Fe}}^{\text{liq}})]$ changes little with temperature or with melt composition, it stays nearly constant at 0.30 ± 0.03 . The equilibrium constant decreases with decreasing SiO_2 or increasing alkalis, and it does increase with increasing pressure. These experiments were conducted by Roeder and Emslie (1970), and their model for $K_D(\text{Fe-Mg})^{\text{ol-liq}} = 0.30$ does stand for basaltic systems, generally at $P < 2\text{-}3$ GPa.

Olivine-liquid thermometers were originally based on Ni partitioning by Hakli and Wright (1967), but many of them showed a high SEE. Later experiments turned to the partitioning of Mg between olivine and liquid. Among all published models for olivine-liquid thermometers there is one superior model by Beattie (1993), equation (19). Where $D_{\text{Mg}}^{\text{ol/liq}}$ is a cation fraction ratio that describes the partition of Mg between olivine and the liquid, the model works also when $D_{\text{Mg}}^{\text{ol/liq}}$ is calculated from the liquid composition so equation (19) can be used without an olivine composition. For that to work, Beattie's (1993) expression for $D_{\text{Mg}}^{\text{ol/liq}}$ must be substituted into equation (19), which gives us equation (20).

The combination of equations (19) and (20) provides very accurate predictions for olivine equilibrium temperatures. Systematic errors do occur in this model at very high temperatures and pressures but Herzberg & O'Hara (2002) provided corrections for these errors. This model also overestimates temperature for hydrous bulk compositions. Equations (21) and (22) were then presented to rectify this issue and integrate corrections made by Herzberg & O'Hara (2002).

The most precise equations are thought to be equations (19) and (22). For anhydrous conditions, equation (19) provides the best estimates, and equation (22) is best for situations when water is present. These thermometers are calibrated with different experimental data but do have similar errors when using test data, so the difference in their estimates is thought to be calibration error. It is therefore, in such cases, no disadvantage in using both equations and averaging the results (Putirka, 2008).

3.3.3 Plagioclase- and alkali feldspar-liquid thermobarometers

The first plagioclase-liquid geothermometer was presented by Kudo and Weill (1970). When Putirka's (2005b) review on these thermometers came out it showed that the

calibration of Sugawara (2001), and the MELTS/pMELTS models of Ghiorso et al. (2002) predict most accurately the T. But these models had problems at low T (<1100 °C) and in case of hydrous systems. Improvements in temperature estimation was obtained from a simpler model by Putirka (2008), equation (23). In this model mineral components are all calculated as cation fractions and all liquid components are calculated on an anhydrous basis without renormalization of weight percent values. According to Putirka (2008) the recalibration yields a ~6 °C improvements in the SEE and the provides equation (24a). By comparing the required temperature for a liquid reaching plagioclase saturation to the temperature from equations (23) and (24a) one can improve precision by 10 °C. Equation (26) determines the temperature plagioclase crystallizes at a given pressure in a silicate liquid. The Ab-An exchange or equilibrium constant (K_D) for these equations is $0,27 \pm 0.11$ at $T > 1050$ °C (Putirka, 2008).

3.4 Re-equilibration of melt inclusions

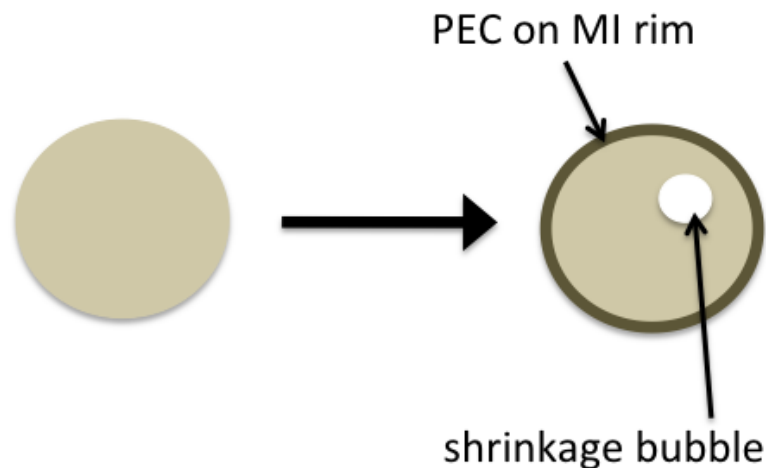


Figure 7: Schematic representation of post entrapment crystallization (PEC). The melt inclusion crystallizes along the interface with the crystal and decreases in volume. This process can create a shrinkage bubble (UO BLOGS, 2016).

Melt inclusions in phenocrysts can potentially undergo a process of post entrapment crystallization. In magnesian olivine (Fo) this results in a process referred to as Fe-loss. When a melt inclusion starts to cool after being trapped it starts to crystallize the host mineral on the inclusion wall, at the contact with the host. Besides crystallization Fe and Mg might be exchanged between the melt inclusion and the host mineral by diffusion. This process can happen during natural pre-eruptive cooling of the host magma and lowers FeO^t contents within the melt inclusion while the MgO content increases. Compositions in glassy inclusions that have undergone Fe-loss will inherit artificially low FeO^t contents and low MgO because of higher Mg# of the residual melt in re-equilibrated inclusions. When there are large temperature intervals of cooling in the magma it can enhance the extent of Fe-loss. From observations of melt inclusions in olivine phenocrysts in several subduction related suits the following observations were noted, 1) Fe-loss is a common process, 2) maximum observed degree of re-equilibration varies between suits, and 3) in a single sample variable degrees of post entrapment crystallization in melt inclusions can be

recorded in phenocrysts of identical composition. Three cases of this are described by Danyushevsky et al. (2000): melt inclusions not affected, inclusions affected by complete post entrapment re-equilibration, and inclusions partially affected. They also demonstrate that this process is fast and it is completed within two years (Danyushevsky et al, 2000). When it comes to mantle-derived magmas, inclusions in high-Fo phenocrysts are most often partially re-equilibrated at temperatures below trapping. Partial re-equilibration, meaning diffusion of Fe out of and Mg into the initial volume. Factors determining the extent of this process are cooling interval before eruption ($<350^{\circ}\text{C}$), eruption temperatures ($>1000^{\circ}\text{C}$), and inclusion size ($<70\mu\text{m}$ in radius). This means short residence time for high-Fo phenocrysts and suggests that if eruption does not happen within few months after a primitive magma starts cooling and crystalizing, then the olivine that crystalize from it, most likely, do not erupt as phenocrysts. The explanation for this is that there is efficient separation of olivine crystals from the melt, and they incorporate very fast into the cumulate of the chamber. When eruptions happen so soon after cooling starts it helps the high-Fo phenocrysts to retain their original compositions, and protects the composition of melt inclusions from irreversible changes. This means that the cumulate layers of the magmatic system is the main source of high-Fo crystals in erupted magmas. Olivine-phyric rocks are therefore a mixture of an evolved transporting magma with crystals from more primitive melt (Danyushevsky et al, 2002).

4 Results

4.1 Petrography

The troctolite xenolith measures at ~15 cm in diameter and is embedded in a mass of fully crystallized ankaramite. It is crystalline, coarse grained with no groundmass and is built up almost entirely of euhedral or subhedral plagioclase and olivine with small amount of pyroxene, giving the xenolith lighter colouring than its host. Plagioclase and olivine crystals vary in size but are at average ~1-2 mm with no preferred orientation or layering. Cumulate and poikilitic textures can be seen in the rock with neither plagioclase nor olivine showing to be the dominant cumulus phase. Pyroxenes are few in number and show clear evidence of being of an intercumulus phase. Fine-grained melt inclusions are fairly common and can be seen within these minerals as greyish to black “bubbles” with 1 polarizer, varying in shape and size. In the plagioclase hosted melt inclusions there was usually a dark shadow around the inclusion with reflected light which shows its shape under the surface. Figure 8 shows pictures of the troctolite taken by the polarization microscope and SEM, more images can be found in appendix D.

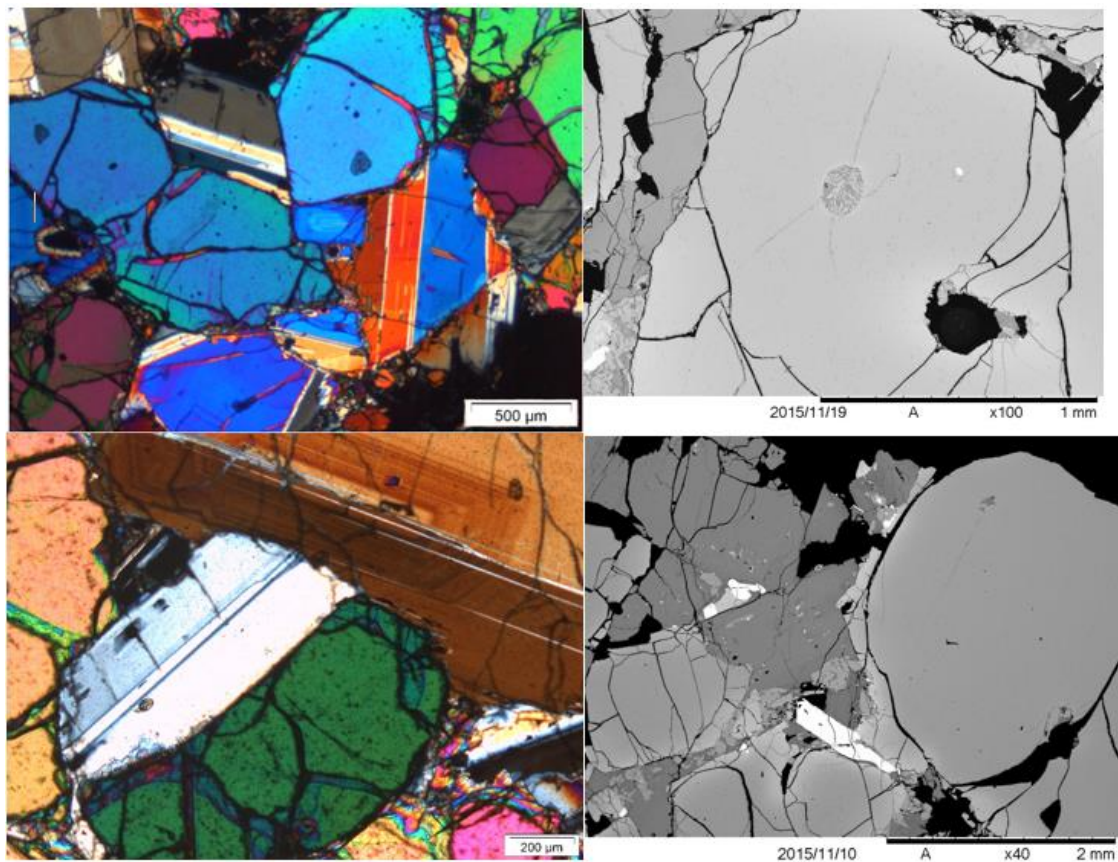


Figure 8: Images from the microscope (left, crossed polarized light) and SEM (right) of the minerals and melt inclusions in the troctolite. Note, the high interference colours of plagioclase is due to a larger than 30 µm thickness of the thin section.

4.2 Chemical analyses

Two of the thin sections were subjected to the SEM after they had been cleaned and carbon coated. The samples had already been mapped out using the petrographic microscope, and places of interest were found. In total 104 chemical analyses were carried out with the SEM on two of the three thin sections available and three chemical maps were made. Chemical analyses were done on olivine, plagioclase, pyroxene and melt inclusions those results will be described here. Analyses were also done on oxide minerals and spinel but those results will not be described here.

4.2.1 Olivine

When there was clear visual evidence of difference between core and rim, in an olivine that was being analysed, two point analyses were made to show the difference, figure 9 shows an example of this. The olivine compositions ranges from Fo_{51.8}-Fo_{82.7}. Differences in core and rim seem to be that FeO increases from the core to the rim by ~10 wt.% while MgO decreases, respectively. Table 1 shows the chemical analyses for olivine and molar percentages for Fo-Fa.

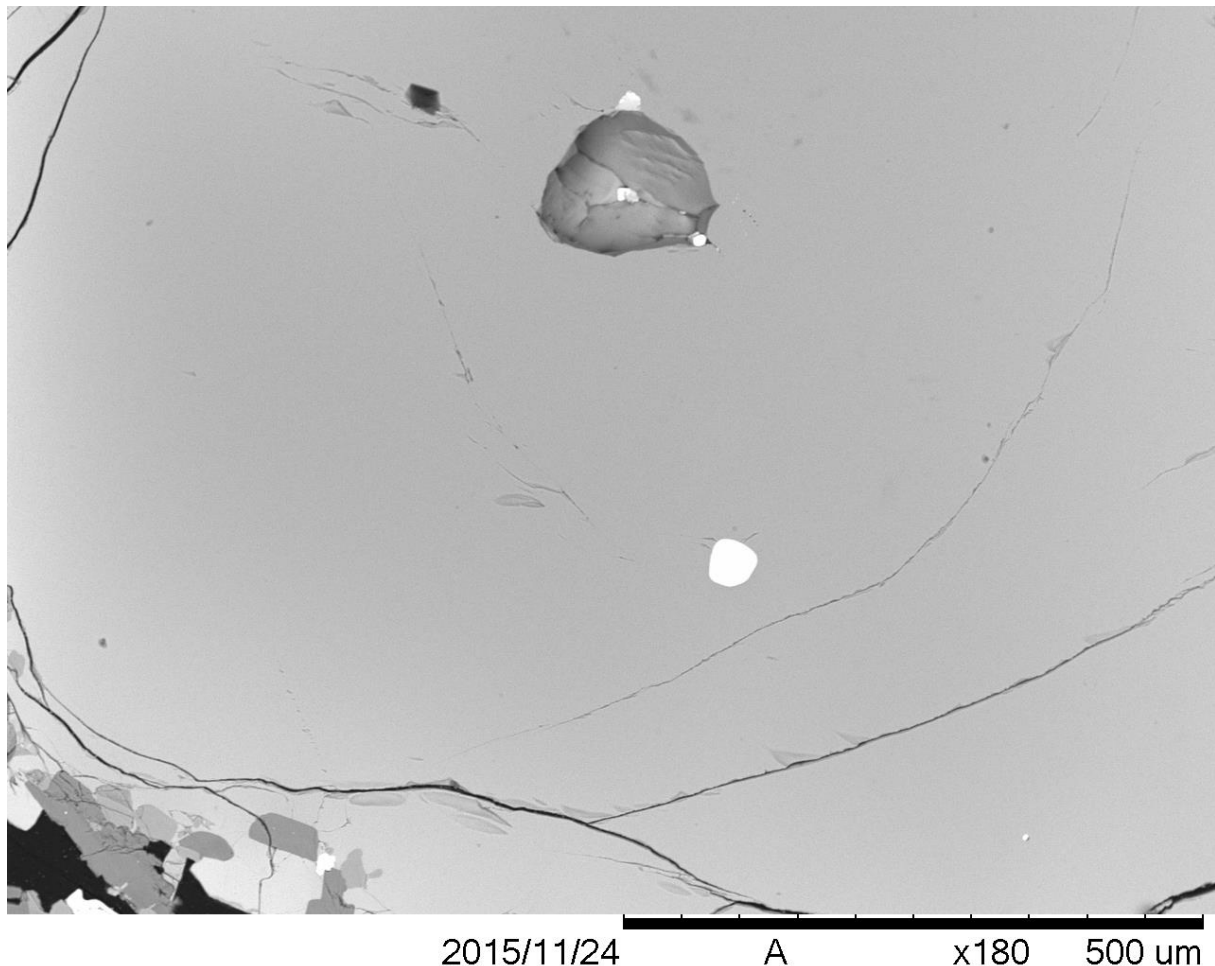


Figure 9: BSE image of olivine showing a darker core with lighter rims. Note the oxide inclusion in the core.

The olivine marked as ts2-o1c and ts2-o1r was found at the contact with the host rock and showed abnormal analyses compared to other samples taken within the troctolite, the core is much richer in MgO and poorer in FeO than other olivine analysed, while the rim shows to be much poorer in MgO and richer in FeO compared to olivine within the troctolite. Olivine within the troctolite have FeO in the range of 20.16-33.83 wt.%, MgO measuring 30.45-41.32 wt.%, and a Mg# in the range of 61.6-78.2.

Table 1: Chemical composition of olivines

Samples	SiO₂	FeO	MnO	MgO	Total	Fo	Fa
ts1-oc1	37.38	21.31	0	41.32	100.01	77.57	22.44
ts1-or1	33.66	31.58	0	34.77	100.01	66.26	33.75
ts1-o2c	37.6	23.05	0	39.35	100	75.28	24.73
ts1-o2r	36.2	31.52	0	32.28	100	64.62	35.39
ts1-o2r2	36.12	30.42	0	33.47	100.01	66.24	33.77
ts1-o3c	37.71	23.14	0	39.15	100	75.11	24.9
ts1-o3r	35.81	32.23	0	31.97	100.01	63.89	36.12
ts1-o4c	37.87	22.45	0	39.69	100.01	75.92	24.09
ts1-o4r	35.73	33.83	0	30.45	100.01	61.62	38.4
ts1-o5	37.59	22.88	0	39.53	100	75.5	24.51
ts1-o6c	39.33	20.16	0	40.52	100.01	78.19	21.82
ts1-o6r	36.46	28.96	0	34.59	100.01	68.05	31.96
ts1-o7c	37.51	23.41	0	39.09	100.01	74.86	25.15
ts1-o7r	35.44	33.56	0	31.01	100.01	62.23	37.78
ts1-o8	37.68	22.87	0	39.46	100.01	75.48	24.54
ts2-o1c	38.18	16.77	0	45.06	100.01	82.74	17.27
ts2-o1r	34.74	39.88	0.84	24.54	100	51.79	47.2
ts2-o2	37.84	22.75	0	39.42	100.01	75.55	24.46
ts2-o3	37.81	22.72	0	39.48	100.01	75.61	24.4
ts2-o4c	38.07	22.15	0	39.79	100.01	76.21	23.8
ts2-o5	36.27	30.83	0	32.9	100	65.56	34.46

Kjartan Björgvin Kristjánsson (2015) did a study on the compositions of host rock olivines. Only six samples were analysed but they do have similar Fo content as olivine in the troctolite. Additional data on the olivine in the host rock was provided by Enikő Bali. Figure 10 shows a histogram with these results.

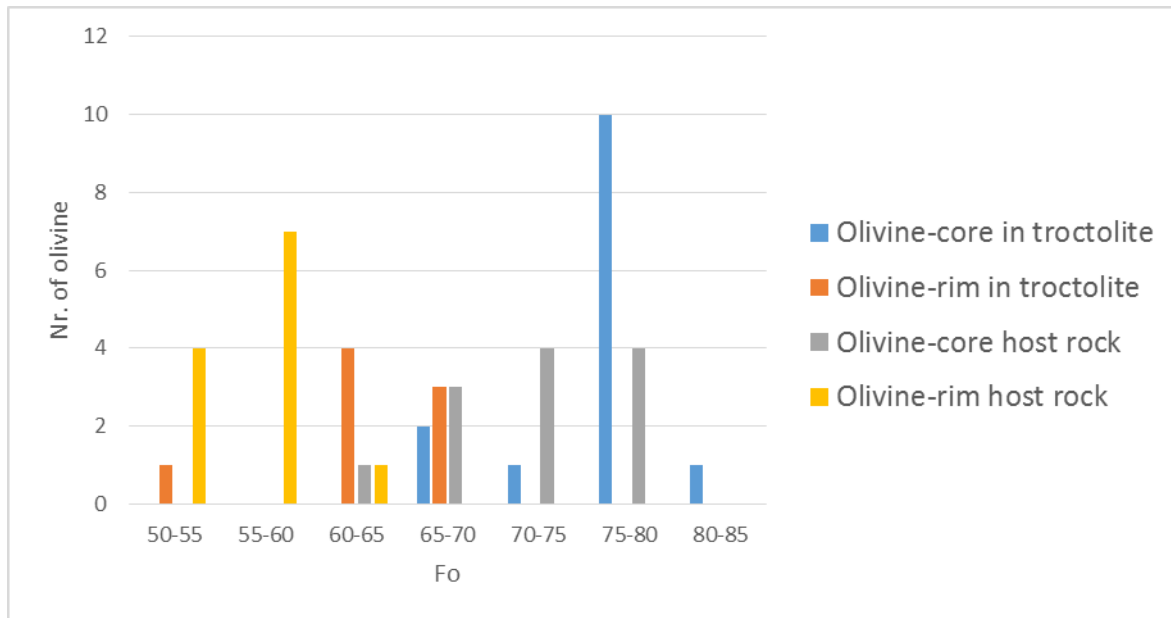
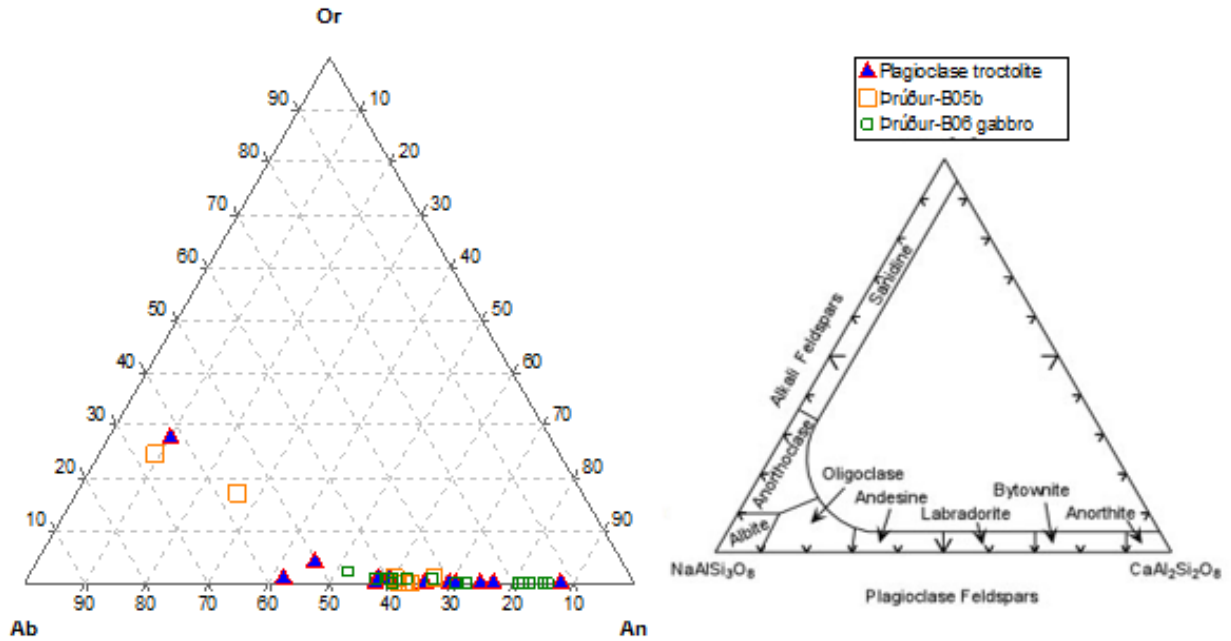


Figure 10: Comparison of olivine in the troctolite and olivine from the host rock. Comparative data from Kristjánsson (2015) and Enikő Bali. The histogram shows nr. of olivine as a function of Fo contents.

4.2.2 Plagioclase

Zonation was noticed in plagioclase while looking at the thin sections in a microscope but were not as clear in the SEM. This led to the decision to only analyse core compositions of plagioclase. In total there were 14 analyses made.

Figure 11 shows a ternary diagram of the plagioclase compositions in the troctolite along with data from a study on plagioclase in the host rock made by Þrúður Helgadóttir (2016). This shows that most of the plagioclase are labradorite and bytownite that are common in mafic igneous rock.



**Figure 11: Ternary diagram showing plagioclase compositions in the troctolite and host rock.
Comparative data are from Helgadóttir (2016)**

Two of the plagioclase are andesine and one is an alkali feldspar called anorthoclase. Sample ts1-plag3 is analysed as an alkali feldspar, the reason for this might be it being placed so close to a melt inclusion that it interferes with the analyses. Other plagioclase varies in composition with An_{41.8}-An_{87.4}. The plagioclase with the highest An content is very narrow and is situated between an olivine and an oxide. Al₂O₃ and CaO are clearly most variable with ranges from 26.64-36.15 wt.% and 9.39-18.77 wt.%, respectively. Table 2 shows the chemical analyses for plagioclase and the molar percentage of An-Ab-Or.

Table 2: Chemical compositions of plagioclases.

Samples	SiO₂	Al₂O₃	FeO	MgO	CaO	Na₂O	K₂O	Total	An	Ab	Or
ts1-plag-1b	49.48	31.57	0	0.19	16.29	2.81	0	100.34	76.21	23.79	0
ts1-plag-c1	47.56	33.73	0	0.68	14.17	4.09	0.12	100.35	65.26	34.09	0.66
ts1-plag-1	56.92	26.64	0	0.37	9.6	6	0.73	100.26	45.01	50.91	4.08
ts1-plag-p3	51.43	31.03	0	0.19	15.02	3.45	0	101.12	70.64	29.36	0
ts1-plag-p4	50.59	31.82	0	0.19	14.94	3.58	0	101.12	69.75	30.25	0
ts1-plag1-p2	48.41	33.49	0	0.5	13	5.36	0	100.76	57.27	42.73	0
ts1-plag2-c	50.18	31.4	0	0.42	13.07	4.91	0.23	100.21	58.8	39.97	1.23
ts1-plag2-p2	49.84	31.08	0	0.19	15.99	3.04	0	100.14	74.4	25.6	0
ts1-plag3	64.12	21.23	0.31	0.36	2.2	7.06	4.82	100.1	10.62	61.67	27.7
ts1-plag4	46.12	36.15	0	0.53	14.89	3.42	0	101.11	70.64	29.36	0
ts2-plag1	45.38	35.54	0	0.58	16.22	2.8	0	100.52	76.2	23.8	0
ts2-plag2	55.07	28.49	0	0.19	9.39	7.05	0.29	100.48	41.75	56.72	1.54
ts2-plag3	46.34	33.32	0	0.35	18.77	1.5	0	100.28	87.37	12.63	0
ts2-plag4	54.19	28.3	0	0.36	12.18	4.86	0.32	100.21	57.03	41.18	1.78

The plagioclase in the troctolite were compared to plagioclase from the host rock, figure 12 shows this comparison. This shows that for both studies that majority of the samples lie in the range of An₅₀-An₈₀. The gabbro xenolith shows lower An contents than the plagioclase in the troctolite, but An content is higher in the host rock than in the troctolite. An₅₀₋₆₀ in the host rock is probably from measurements done at the rim of a plagioclase or near a melt inclusion, while An₈₀₋₉₀ are probably from measurements on core samples.

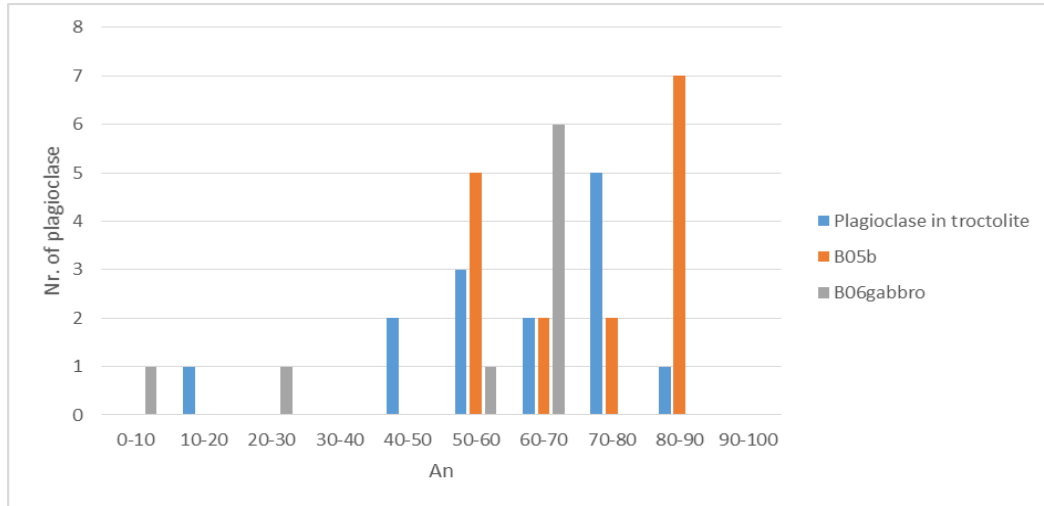


Figure 12: Comparison of plagioclase in the troctolite and plagioclase from the host rock. Comparative data from Helgadóttir (2016). The graph shows nr. of plagioclase as a function of An content.

4.2.3 Pyroxene

In total there were ten pyroxene analyses carried out by the SEM from the two thin sections. Table 3 shows the chemical compositions and the molar percentage for Fs-En-Wo.

Figure 13 shows a ternary diagram with the pyroxene compositions and a standard classification diagram for pyroxene. If those diagrams are compared, it seems that most of the pyroxene cluster at the border between augite and diopside.

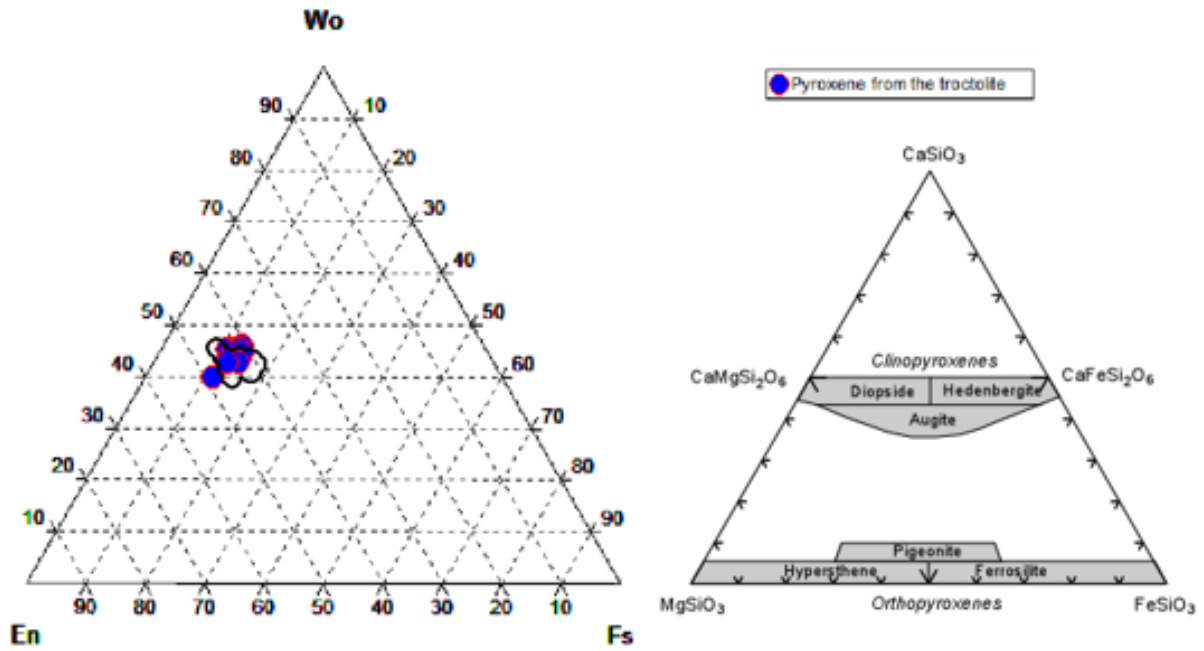


Figure 13: Ternary diagram showing pyroxene compositions in the troctolite. The black circle represents pyroxenes from the host rock analysed by Gísladóttir (2015).

The pyroxene seem to be homogeneous with CaO being the most prominent component with a range of 19.41-21.77 wt.% with the average being 21.01 wt.%. MgO comes next with a range of 13.83-16.97 wt.% and FeO being ca. half of the MgO percentage, ranging from 7.14-9.12 wt.%. This gives an Mg# in the span of 74.3-80.2 averaging at 76.6. Al₂O₃ content varies from 1.94-6.32 wt.%, which is significant for pyroxene.

Table 3: Chemical compositions of pyroxenes.

	Samples									
	ts1- pyr1	ts1- pyr	ts1- pyr2b	ts1- pyr3	ts1-pyr4	ts1- pyr5	ts2- pyr2	ts2- pyr3	ts2- pyr4	ts2- pyr5
SiO₂	50.80	50.90	50.48	49.85	48.81	48.15	48.49	49.79	51.72	51.24
TiO₂	1.55	1.63	1.27	1.37	1.64	1.91	1.74	1.76	1.22	1.70
Al₂O₃	3.00	2.22	4.08	4.76	5.66	6.32	6.28	3.87	1.94	2.91
FeO	7.49	9.12	7.14	7.41	7.91	7.96	8.05	8.83	9.10	7.84
MnO	0.00	0.00	0.00	0.00	0.00	0.00	0.00	0.00	0.00	0.00
MgO	16.97	14.76	15.09	14.67	14.44	13.83	14.05	14.33	14.96	15.51
CaO	19.41	21.12	21.77	21.77	21.11	21.55	21.12	21.18	20.76	20.34
Na₂O	0.79	0.26	0.17	0.17	0.43	0.28	0.28	0.25	0.31	0.47
K₂O	0.00	0.00	0.00	0.00	0.00	0.00	0.00	0.00	0.00	0.00
Total	100.01	100.01	100.00	100.00	100.00	100.00	100.01	100.01	100.01	100.01
Wo	39.77	43.33	45.06	45.41	44.61	45.89	45.02	44.15	42.67	42.36
En	48.39	42.14	43.46	42.58	42.46	40.98	41.67	41.56	42.78	44.95
Fs	11.84	14.54	11.48	12.00	12.93	13.14	13.31	14.29	14.55	12.70
Mg#	80.20	74.30	79.00	77.90	76.50	75.60	75.70	74.30	74.60	77.90

The pyroxenes were compared to samples from the host rock, analysed by Bryndís Ýr Gísladóttir (2015), and two histograms were made to show the comparison, figures 14 and 15. The histograms show similar compositional range of the pyroxenes in the troctolite and in the host rock, where most of the pyroxene are in the Mg# range of 72-78 and their numbers decrease with higher Mg#.

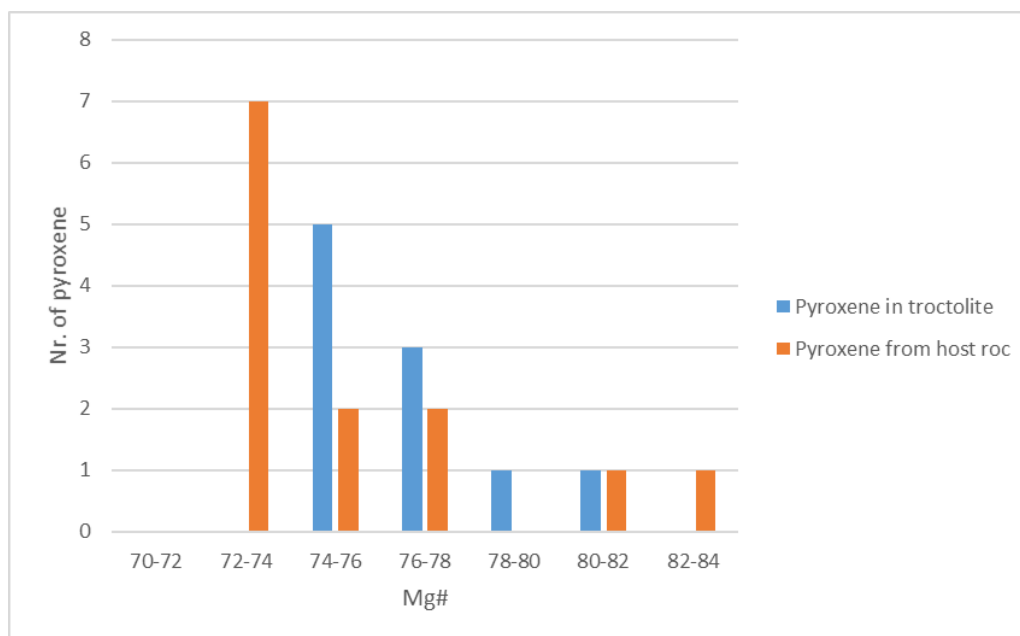


Figure 14: Comparison of pyroxene in the troctolite and pyroxene from the host rock. Comparative data from Gísladóttir (2015). The graph shows nr. of pyroxene as a function of Mg#.

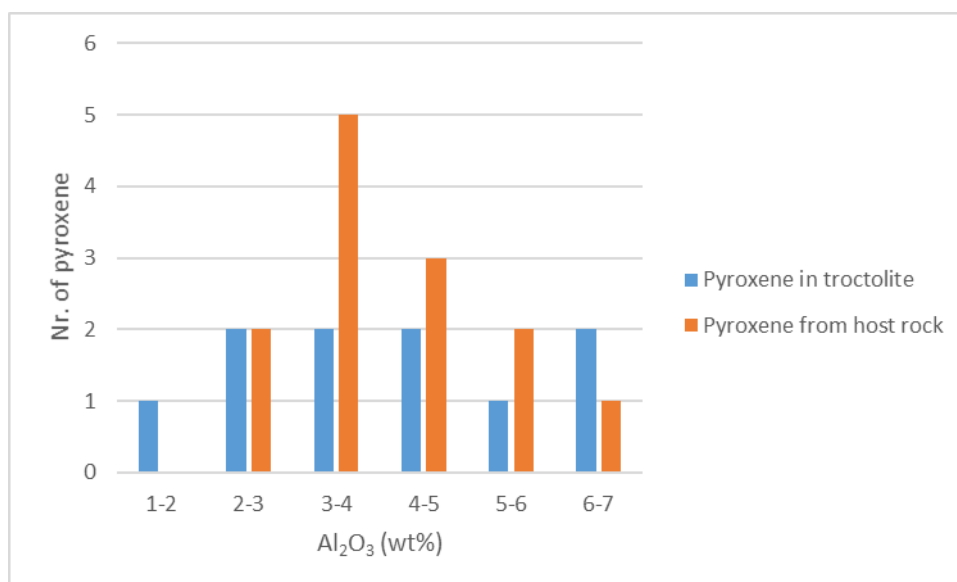


Figure 15: Comparison of pyroxene in the troctolite and pyroxene from the host rock. Comparative data from Gísladóttir (2015). The graph shows nr. of pyroxene as a function of Mg#.

4.2.4 Melt inclusions

Total of 12 melt inclusions were analysed from the two thin sections and they were found both in plagioclase and olivine. Because the inclusions probably went through changes after being trapped, in form of post entrapment crystallization (PEC), they had to be re-equilibrated to obtain the composition of the original melt.

The raw chemical analyses are shown in appendix B and table 4 shows the results after post entrapment corrections. For olivine hosted melt inclusions a program called Petrolog3 was used for the re-equilibration calculations, it is provided by Danyushevsky & Plechov (2011) and is available on the internet. It takes measured chemical composition of the melt inclusion, Fo content of the host olivine, and FeO^* that needs to be calculated. Oxidation state also needs to be decided, it was set as equal to QFM. In order to determine FeO^* , olivine hosted melt inclusions compositions from Moune et al. (2012), melt inclusions from plagioclase measured here and groundmass compositions of Kristjánsson (2015) were used. These melt compositions were plotted on a graph showing FeO against TiO_2 . Melt inclusions in plagioclase and groundmass compositions as well as most of the olivine hosted melt inclusions from Moune et al. (2012) fall on a single trend, whereas some of the olivine hosted melt inclusions measured in this study were off this trend. Trend line was fitted for the plagioclase hosted melt inclusions and the groundmass and from its equation FeO^* was calculated for olivine hosted melt inclusions.

For plagioclase hosted melt inclusions the re-equilibration had to be done by hand. Similar graph as before was made but now Al_2O_3 in the melt inclusions was plotted up against TiO_2 , from the trend line equation it was possible to calculate the original concentrations for Al_2O_3 and decide how much re-equilibration was needed. From these results it was found that 25% re-equilibration was needed for all but two of the samples, they seemed to not need any re-equilibration and were kept as they were. Graph showing the trend of re-equilibration from 0-25% can be found in appendix C. Figure 16 shows a Total alkali-silica diagram (TAS) for the melt inclusions before and after PEC.

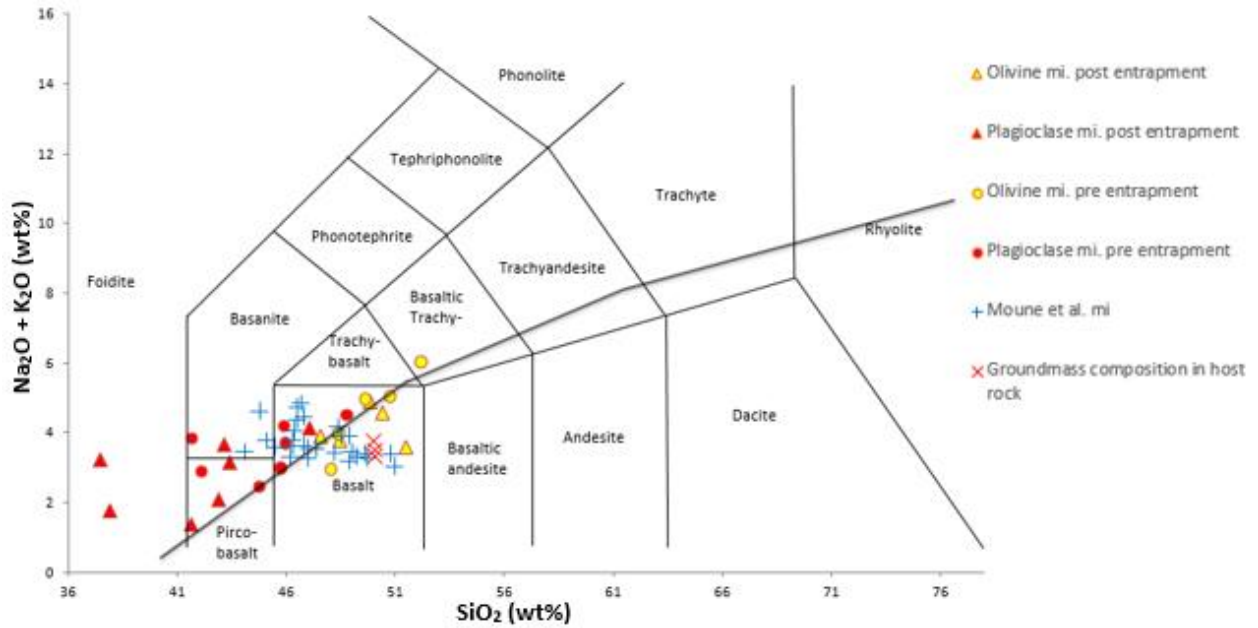


Figure 16: TAS diagram for melt inclusions before (triangles) and after (dots) post entrapment correction. mi. stands for melt inclusions.

Table 4 shows Mg# of the melt inclusions in the range of 33.86-51.69 showing that the parental magma of troctolite was fairly evolved. If one looks only at melt inclusions from olivine the range is much narrower and the Mg# there spans 45-47. Figure 17 shows comparison of some components in the studied melt inclusions along with melt inclusions in olivine from Fimmvörðuháls 2010 flank eruption calculated by Moune et al. (2012), and the groundmass compositions of the host rock by Kristjánsson (2015). The melt inclusions are in general really homogenous, with one to four analyses sometimes going off trend. This can be seen in the concentration for Al_2O_3 , ranging from 11.38-18.75 wt.% with an average of 14.59 wt.%, and CaO that ranges from 10.04-15.21 wt.% and averages at 11.93 wt.%. This might be due to analytical uncertainty.

Table 4: Re-equilibrated compositions of melt inclusions. Blue samples are plagioclase hosted and green samples are olivine hosted.

Samples	SiO ₂	TiO ₂	Al ₂ O ₃	FeO	MnO	MgO	CaO	Na ₂ O	K ₂ O	P ₂ O ₅	Fe ₂ O ₃	Total	Mg#
plag1 incl1	45.78	3.92	12.67	15.32	0.03	7.98	11.23	2.57	0.40	0.23		100.13	48.15
incl plag3	42.15	5.42	11.36	16.16	0.03	4.64	15.21	2.41	0.47	2.36		100.21	33.86
mi1	41.70	7.46	12.17	15.72	0.44	5.44	12.10	3.33	0.50	1.25		100.11	38.16
mi2	47.05	5.94	17.01	8.76	0.27	3.54	12.77	3.51	0.62	0.53		100.00	41.9
plag2 incl	43.13	5.18	12.87	18.29	0.04	6.71	10.04	3.11	0.55	0.07		99.99	39.5
incl3 plag4	44.83	4.23	11.74	16.60	0.03	8.95	11.19	2.13	0.31	0.11		100.12	49.01
incl2 plag4	46.03	3.92	13.36	13.28	0.39	7.97	11.20	3.15	0.50	0.21		100.01	51.69
mi3	50.78	3.22	16.38	7.63	0.04	4.47	10.85	4.31	0.68	0.12	1.52	100.00	46.6
incl olivine4	48.47	2.70	18.24	6.89	0.04	3.82	14.55	2.27	1.66	0.04	1.33	100.01	45.3
incl olivine6	49.67	3.58	17.51	7.33	0.05	4.38	11.01	4.14	0.78	0.05	1.49	99.99	47.0
incl1 ol4	52.25	2.47	18.75	5.54	0.05	3.03	10.72	3.81	2.19	0.15	1.06	100.02	45.0
incl2 ol4	48.06	3.54	13.06	10.91	0.03	6.32	12.30	2.06	0.84	0.75	2.13	100.00	46.4

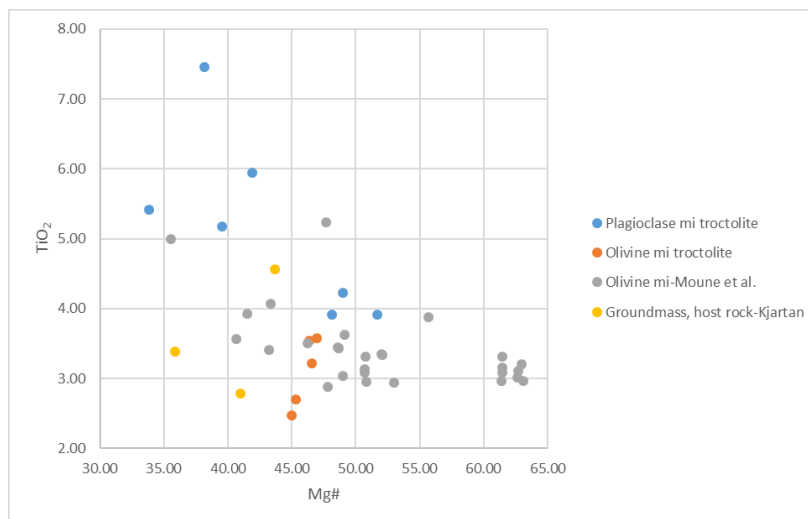
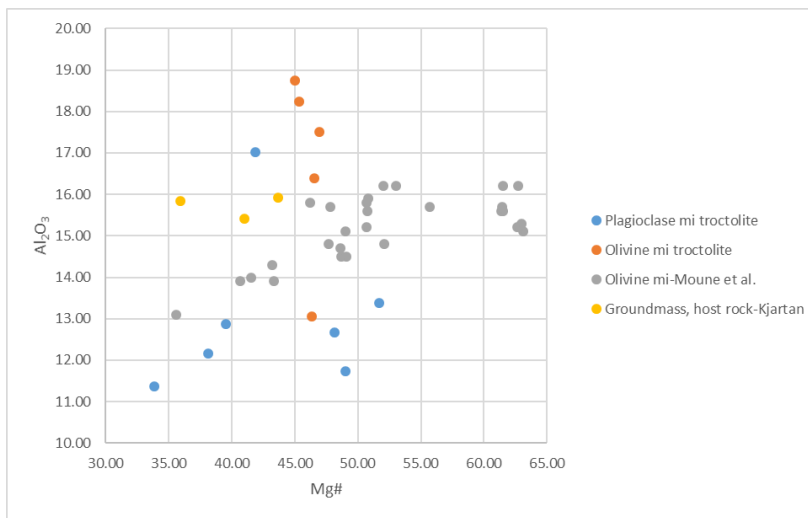
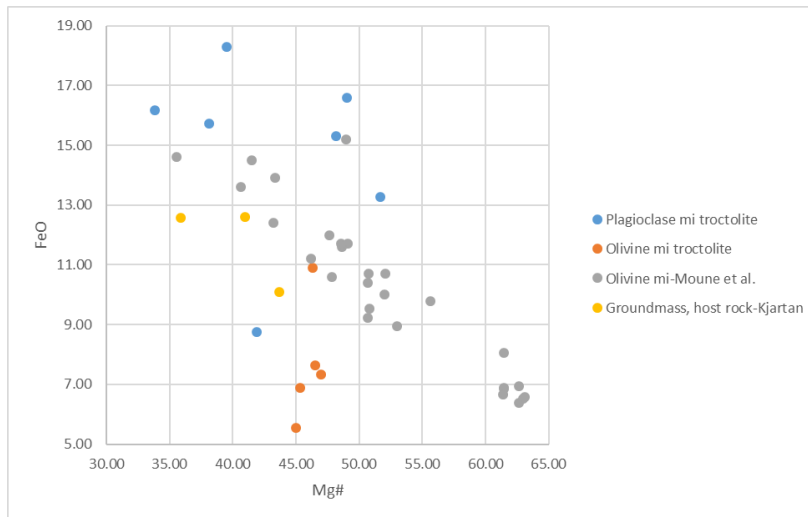


Figure 17: Comparison of the wt.% for SiO_2 , FeO, and Al_2O_3 as a function of Mg# in the melt inclusions.

4.3 Thermal calculations for melt inclusions

Table 5 shows the results for thermal calculations in olivine hosted melt inclusions. Since the mineral assemblage clearly indicate that the xenolith has a crustal origin, a crustal pressure of 0.5 GPa was used for thermal calculations. Note the pressure effect is minor on these thermometers as demonstrated by Kristjánsson (2015). When K_D falls into the range of 0.3 ± 0.03 it is assumed that the inclusion is in chemical equilibrium with its host. Most of the olivine hosted inclusions fell into that range except one, incl olivine4, that inclusion was not included in the average calculations. Equation (14) shows the lowest average temperature of $1112 \pm 50^\circ\text{C}$ and equation (15) has the highest average temperature of $1138 \pm 60^\circ\text{C}$. According to Putirka (2008), equations (19) and (20) show the most precise estimates for these equations, and their average show temperature of $1116 \pm 45^\circ\text{C}$. All calculations are within the uncertainty of the different calibrations.

Table 5: Results for the thermal calculations in olivine hosted melt inclusions. Showing for fixed pressure of 0.5 GPa. K_D is green if chemical equilibrium can be assumed (it falls into the range of 0.3 ± 0.03).

Sample	Equation (13) T(°C)	Equation (14) T(°C)	Equation (15) T(°C)	Equation (19) T(°C)	Equation (22) T(°C)	Mesured K_D (Fe-Mg)
mi3	1112	1113	1138	1119	1118	0.302
incl olivine4	1095	1071	1111	1057	1086	0.339
incl olivine6	1110	1108	1135	1111	1116	0.297
incl1 ol4	1074	1068	1100	1052	1059	0.304
incl2 ol4	1161	1160	1180	1170	1183	0.322
Average	1114	1112	1138	1113	1119	
SEE	$\pm 71^\circ\text{C}$	$\pm 50^\circ\text{C}$	$\pm 60^\circ\text{C}$	$\pm 31^\circ\text{C}$	$\pm 45^\circ\text{C}$	

Table 6 shows the results for thermal calculations in plagioclase hosted melt inclusions. Those inclusions that do not fall into the desirable K_D range, 0.27 ± 0.11 for plagioclase hosted melt inclusions, are not included in the calculations. Similarly as for olivine hosted inclusions an input pressure of 0.5 GPa was used. Equation (26) shows the temperature of plagioclase crystallization should occur at average T of $1137 \pm 37^\circ\text{C}$. The other equations show a combined average of $1177 \pm 43^\circ\text{C}$.

Figure 18 shows a graph of average thermal calculations for all equations, both in olivine and plagioclase hosted melt inclusions, along with the measured SEE for each equation.

Table 6: Results for the thermal calculations on plagioclase hosted melt inclusions. Showing for fixed pressure of 0.5 GPa. K_D is green if chemical equilibrium can be assumed (it falls into the range of 0.27 ± 0.11).

Pressure (Gpa)	0.5			
Sample	Equation (23) T(°C)	Equation (24a) T(°C)	Equation (26) T(°C)	Mesured K_D (Ab-An)
plag1 incl1	1175	1144	1112	0.25
incl plag3	1216	1182	1145	0.16
mi1	1192	1166	1130	0.22
mi2	1303	1245	1291	0.43
plag2 incl	1229	1194	1197	0.45
incl3 plag4	1164	1165	1137	0.37
incl2 plag4	1189	1180	1159	0.28
Average	1187	1167	1137	
SEE	$\pm 43^\circ\text{C}$	$\pm 36^\circ\text{C}$	$\pm 37^\circ\text{C}$	

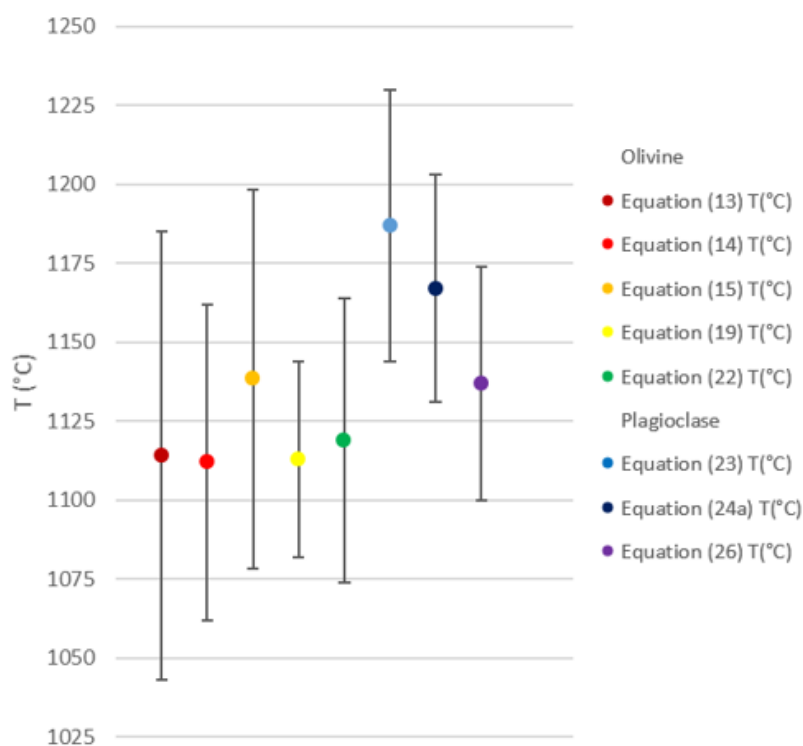


Figure 18: Graph showing thermal calculations in olivine and plagioclase hosted melt inclusions with the SEE for each equation.

5 Discussion

The purpose of this thesis was to chemically analyse the minerals and melt inclusions in the troctolite from Hamragarðabeiði and by utilizing thermometers from Putirka (2008) try to determine the temperature of crystallization for the parental magma. Also to compare those results to other works of similar nature. The uniqueness of Icelandic magmatism has become a focus for mid-ocean ridge specialists and the investigation of magmatic processes. The reason for that is it is an island sitting on a spreading ridge and has unusually high mantle melt producing rate. These formations can be well studied due to great exposure at some places (Sigmarsson et al. 2008).

5.1 Chemical analyses

Some of the olivine in the troctolite is MgO richer and FeO poorer than those in the host rock which shows that it is from an early crystallisation. Fo percentages in cores and rims show similar distribution for both rocks, as is seen in figure 10. This similarity suggests that they come from the same or very similar original melt.

The plagioclase in the host rock and troctolite are very homogeneous where the troctolite shows slightly more concentration of Al_2O_3 in some cases. CaO concentrations in plagioclase of both rocks show exactly the same trend which reinforces the proposed connection between the xenolith and the host rock.

Pyroxene in the troctolite shows a little more concentration of CaO compared to those in the host rock, and that is supported by more production of diopside, as can be seen in figure 13, but in general the pyroxene in the xenolith and the host rock are also very similar.

The melt inclusions are primarily basalts on the TAS diagram (figure 16), and sit on the division line for alkaline sub-alkaline series. When comparing the melt inclusions in the troctolite to the groundmass in the host rock and melt inclusions from Fimmvörðuháls, one can see the similarities in chemical trends between them. These chemical similarities suggest similar parental melt compositions for all of them.

5.2 Thermal calculation

Most of the melt inclusions after PEC corrections show to be in equilibrium with their host. Those measurements who fall out of the zone of equilibration were not used for the final results. Table 5 shows results for the olivine melt inclusion thermometer. Putirka (2008) states that the most precise equations to be (19) and (22). If one looks only at those results the temperature is in the range of 1113-1119°C and averaging at $1116 \pm 45^\circ\text{C}$. Looking at all the equations (13, 14, 15, 19 and 22) the uncertainty rises but stays in SEE range of the first estimate, the temperature range is 1112-1138°C and averages at $1125 \pm 71^\circ\text{C}$. Comparing these results to thermal calculations on the host rock from Kristjánsson (2015), which show a temperature range of 1108-1134°C and averaging at $1121 \pm 71^\circ\text{C}$ using equations (13), (14), and (15). These temperatures are essentially the same.

Most of the plagioclase hosted inclusions are in equilibrium with their host, those which are not were put aside for the final results. Table 6 shows results for the plagioclase melt inclusion thermometer. Equation (26) shows the temperature of crystallization should occur at an average of $1137 \pm 37^{\circ}\text{C}$. Results from equations (23) and (24a) show a range of $1167\text{-}1187^{\circ}\text{C}$ and averages at $1177 \pm 43^{\circ}\text{C}$.

Comparing results from the olivine hosted and plagioclase hosted melt inclusions one can see slightly higher average temperature of crystallization for the plagioclase but the temperatures do stay within the SEE range of each other.

6 Summary and Conclusions

- (1) 104 analyses were performed on two thin sections from the troctolite with the SEM-EDS. Minerals analysed were olivine, plagioclase and pyroxene but the main focus was on analysing the melt inclusions in olivine and plagioclase.
- (2) The olivine's Fo content was measured in the range of Fo_{61.6}-Fo_{78.2}, similar to those observed in the host ankaramite.
- (3) The plagioclase have An content in the range of An_{41.75}-An_{87.37}. Most of them are labradorite and bytownite, two of them are andesine and there was one alkali feldspar. These compositions are similar to those in the host rock.
- (4) The Pyroxene have high MgO concentration in the range of 13.83-16.97 wt.% and a high uniform CaO concentration in the range of 19.41-21.77 wt.%. The FeO concentration ranges from 7.14-9.12 wt.%. these are similar to those in the host rock.
- (5) The melt inclusions corrected for PEC have a Mg# ranging from 33.86-51.69, and showing the ranges in concentration to be, Al₂O₃: 11.36-18.75 wt.%, FeO: 5.54-18.29 wt.%, MgO: 3.03-8.95 wt.%, CaO: 10.04-15.21.
- (6) Comparison between the chemical compositions in the troctolite to chemical compositions in the host rock and at Fimmvörðuháls show much similarities, drawing the conclusion that they might all be from similar parental melt.
- (7) Thermal calculations show that the temperature for crystallization of olivine to be $1116 \pm 45^{\circ}\text{C}$ which corresponds well, and is in SEE range of the plagioclase, that show a temperature of $1177 \pm 43^{\circ}\text{C}$. For the troctolite as a whole, crystallization T is $1147 \pm 45^{\circ}\text{C}$.

References

- Blundi, J. & Cashman, K. (2008). Petrologic Reconstruction of Magmatic System Variables and Processes. *Mineralogy & Geochemistry* 69, 179-239.
- Carleton (2015). Plagioclase feldspar. Retrieved 11 april 2016 from <http://www.people.carleton.edu/~bhaileab/introductiontogeology/Minerals/Plagioclase/Plagioclase.dwt>
- Danyushevsky, L. V., Della-Pasqua, F. N. & Sokolov, S. (2000). Re-equilibration of melt inclusions trapped by magnesian olivine phenocrysts from subduction-related magmas: petrological implication. *Contrib Mineral Petrol*, 138, 68-83.
- Danyushevsky, L. V., Sokolov, S. & Falloon, T. J. (2002). Melt Inclusions in Olivine Phenocrysts: Using Diffusive Re-equilibration to Determine the Cooling History of a Crystal, with Implications for the Origin of Olivine-phyric Volcanic Rocks. *JURNAL OF PETROLOGY*, 43(9), 1651-1671.
- Deer, W.A., Howie, R.A. & Zussman, J. (2013). *An Introduction to the Rock-Forming Minerals*. England: Mineralogical Society.
- Drouin, M., Godard, M., Ildefonse, B., Bruguier, O. & Garrido, C.J. (2009). Geochemical and petrographic evidence for magmatic impregnation in the oceanic lithosphere at Atlantis Massif, Mid-Atlantic Ridge (IODP Hole U1309D, 30°N). *Chemical Geology*, 264, 71-88.
- Einarsson, Á. (2012). *Origin of macrocrysts and gabbro-nodules in Hengill, SW Iceland*. Unpublished MS thesis, University of Iceland, Iceland. pp 41.
- Gísladóttir, B. Ý. (2015). *Pyroxene chemistry in the ankaramite of the hamragarðsheiði quarry, Iceland*. Unpublished BSc thesis, University of Iceland, Iceland. pp 49.
- Gurenko, A. A., Sobolev, A. V. (2006). Crust-primitive magma interaction beneath neovolcanic rift zone of Iceland recorded in gabbro xenoliths from Midfell, SW Iceland. *Contrib Mineral Petrol* 151, 495-520.
- Helgadóttir, Þ. (2016). *Comparative analyses of plagioclase in the Eyjafjöll ankaramites*. Unpublished BSc thesis, University of Iceland, Iceland. pp 64.
- Jakobsson, S. P. (1979). Petrology of Recent basalts of the Eastern Volcanic Zone, Iceland. *Acta Naturalia Islandica* 26, 103p.
- Jakobsson, S. P., Jónasson, K. & Sigurðsson, I. A. (2008). The three igneous rock series of Iceland. *Jökull* 58, 117-138.

- Jakobsen, J. K., Tegner, C., Brooks, C. K., Kent, A. J. R., Leshner, C. E., Nielsen, T. F. D. & Wiedenbeck, M. (2010). Parental magma of the Skaergaard intrusion: constraints from melt inclusions in primitive troctolite blocks and FG-1 dykes. *Contrib Mineral Petrol* 159, 61-79
- Jónsson, J. (1998). *Eyjafjöll: Drög að jarðfræði*. Neðri-Ás: Hveragerði.
- Keiding, J. K. & Sigmarsson, O. (2012). Geothermobarometry of the 2010 Eyjafjallajökull eruption: New constraints on Icelandic magma plumbing systems. *Journal of Geophysical Research* 117, 15p.
- Kristjánsson, K. B. (2015). *Samanburður á bergfræði og kristöllumarhitastigi þriggja hrauna úr Eyjafjallajökli*. Unpublished BSc thesis, University of Iceland, Iceland. pp 37.
- Larsen, G., Pedersen, R. & Ilyinskaya, E. (2012). The flank and summit eruptions 2010. Þorkelsson, B. (editor), *The Eyjafjallajökull eruption, Iceland*. 47.
- Middlemost, Eric A.K. (1985). *An introduction to igneous petrology: Magmas and Magmatic Rocks*. England: Longman Group Limited.
- Morimoto, N. (1988). Nomenclature of Pyroxenes. *American Mineralogist*, vol. 73, 1123-1133.
- Moune, S. Sigmarsson, O. Schiano, P. Thordarson, T. & Keiding, J.K. (2012). Melt inclusion constraints on the magma source of Eyjafjallajökull 2010 flank eruption. *Journal of Geophysical Research*, vol. 117, no. 2.
- Nesse, W. D. (2012). *Introduction to Mineralogy*. New York: Oxford University Press.
- Purdue University (2014). *Scanning Electron Microscope*. Retrieved 20 April 2016 from <https://www.purdue.edu/ehps/rem/rs/sem.htm>
- Putirka, K. D. (2008). Thermometers and Barometers for Volcanic Systems. *Mineralogy & Geochemistry* 69, 61-120.
- Renna, M.R. & Tribuzio, R. (2011). Olivine-rich Troctolites from Ligurian Ophiolites (Italy): Evidence for Impregnation of Replacive Mantle Conduits by MORB-type Melts. *Journal of Petrology*, 52(9), 1763-1790.
- Sandatlas (2016). *Troctolite*. Retrieved 2 May 2016 from <http://www.sandatlas.org/troctolite/>
- Sigmarsson, O., MacLennan, J. & Carpentier, M. (2008). Geochemistry of igneous rocks in Iceland: a review. *Jökull* 58, 139-160.
- Sæmundsson, K. (1980). Outline of the geology of Iceland. *Jökull* 29, 7-28.
- Thordarson, T. & Larsen, G. (2007). Volcanism in Iceland in historical time: Volcanos types, eruptions styles and eruptive history. *Journal of Geodynamics*, vol 43, 118-152.

UO BLOGS (2016). *Ellen Aster University of Oregon*. Retrieved 20 April 2016 from <http://blogs.uoregon.edu/ellenaster/research/>

Appendix A

$$T(^{\circ}\text{C}) = 26.3\text{MgO}^{liq} + 994.4\text{ }^{\circ}\text{C} \quad (13)$$

Figure 19: A screenshot of equation (13) from Putirka (2008).

$$T(^{\circ}\text{C}) = 754 + 190.6[\text{Mg}\#] + 25.52[\text{MgO}^{liq}] + 9.585[\text{FeO}^{liq}] + 14.87[(\text{Na}_2\text{O} + \text{K}_2\text{O})^{liq}] - 9.176[\text{H}_2\text{O}^{liq}] \quad (14)$$

$$T(^{\circ}\text{C}) = 815.3 + 265.5[\text{Mg}\#^{liq}] + 15.37[\text{MgO}^{liq}] + 8.61[\text{FeO}^{liq}] + 6.646[(\text{Na}_2\text{O} + \text{K}_2\text{O})^{liq}] + 39.16[P(\text{GPa})] - 12.83[\text{H}_2\text{O}^{liq}] \quad (15)$$

Figure 20: A screenshot of equations (14) and (15) from Putirka (2008).

$$T(^{\circ}\text{C}) = -583 + 3141[X_{\text{SiO}_2}^{liq}] + 15779[X_{\text{Al}_2\text{O}_3}^{liq}] + 1338.6[X_{\text{MgO}}^{liq}] - 31440[X_{\text{SiO}_2}^{liq} \cdot X_{\text{Al}_2\text{O}_3}^{liq}] + 77.67[P(\text{GPa})] \quad (16)$$

Figure 21: A screenshot of equation (16) from Putirka (2008).

$$T(^{\circ}\text{C}) = \frac{13603 + 4.943 \times 10^{-7} (P(\text{GPa}) \times 10^9 - 10^{-5})}{6.26 + 2 \ln D_{\text{Mg}}^{ol/liq} + 2 \ln[1.5(C_{NM}^L)] + 2 \ln[3(C_{\text{SiO}_2}^L)] - NF} - 273.15 \quad (19)$$

Figure 22: A screenshot of equation (19) from Putirka (2008).

$$D_{\text{Mg}}^{ol/liq} = \frac{0.666 - (-0.049X_{\text{MnO}}^{liq} + 0.027X_{\text{FeO}}^{liq})}{X_{\text{MgO}}^{liq} + 0.259X_{\text{MnO}}^{liq} + 0.299X_{\text{FeO}}^{liq}} \quad (20)$$

Figure 23: A screenshot of equation (20) from Putirka (2008).

$$\ln D_{\text{Mg}}^{\text{ol/liq}} = -2.158 + 55.09 \frac{P(\text{GPa})}{T(^{\circ}\text{C})} - 6.213 \times 10^{-2} [\text{H}_2\text{O}^{\text{liq}}] + \frac{4430}{T(^{\circ}\text{C})} + 5.115 \times 10^{-2} [\text{Na}_2\text{O}^{\text{liq}} + \text{K}_2\text{O}^{\text{liq}}] \quad (21)$$

$$T(^{\circ}\text{C}) = \{15294.6 + 1318.8P(\text{GPa}) + 2.4834[P(\text{GPa})]^2\} / \{8.048 + 2.8352 \ln D_{\text{Mg}}^{\text{ol/liq}} + 2.097 \ln[1.5(C_{\text{NM}}^{\text{L}})] + 2.575 \ln[3(C_{\text{SiO}_2}^{\text{liq}})] - 1.41NF + 0.222\text{H}_2\text{O}^{\text{liq}} + 0.5P(\text{GPa})\} \quad (22)$$

Figure 24: A screenshot of equations (21) and (22) from Putirka (2008).

$$\frac{10^4}{T(\text{K})} = 6.12 + 0.257 \ln \left(\frac{X_{\text{An}}^{\text{pl}}}{X_{\text{CaO}}^{\text{liq}} (X_{\text{AlO}_{1.5}}^{\text{liq}})^2 (X_{\text{SiO}_2}^{\text{liq}})^2} \right) - 3.166 (X_{\text{CaO}}^{\text{liq}}) - 3.137 \left(\frac{X_{\text{AlO}_{1.5}}^{\text{liq}}}{X_{\text{AlO}_{1.5}}^{\text{liq}} + X_{\text{SiO}_2}^{\text{liq}}} \right) + 1.216 (X_{\text{Ab}}^{\text{pl}})^2 - 2.475 \times 10^{-2} (P(\text{kbar})) + 0.2166 (\text{H}_2\text{O}^{\text{liq}}) \quad (23)$$

Figure 25: A screenshot of equation (23) from Putirka (2008).

$$\frac{10^4}{T(\text{K})} = 6.4706 + 0.3128 \ln \left(\frac{X_{\text{An}}^{\text{pl}}}{X_{\text{CaO}}^{\text{liq}} (X_{\text{AlO}_{1.5}}^{\text{liq}})^2 (X_{\text{SiO}_2}^{\text{liq}})^2} \right) - 8.103 (X_{\text{SiO}_2}^{\text{liq}}) + 4.872 (X_{\text{K}_{0.5}}^{\text{liq}}) + 1.5346 (X_{\text{Ab}}^{\text{pl}})^2 + 8.661 (X_{\text{SiO}_2}^{\text{liq}})^2 - 3.341 \times 10^{-2} (P(\text{kbar})) + 0.18047 (\text{H}_2\text{O}^{\text{liq}}) \quad (24a)$$

$$\frac{10^4}{T(\text{K})} = 10.86 - 9.7654 (X_{\text{SiO}_2}^{\text{liq}}) + 4.241 (X_{\text{CaO}}^{\text{liq}}) - 55.56 (X_{\text{CaO}}^{\text{liq}} X_{\text{AlO}_{1.5}}^{\text{liq}}) + 37.50 (X_{\text{K}_{0.5}}^{\text{liq}} X_{\text{AlO}_{1.5}}^{\text{liq}}) + 11.206 (X_{\text{SiO}_2}^{\text{liq}})^3 - 3.151 \times 10^{-2} (P(\text{kbar})) + 0.1709 (\text{H}_2\text{O}^{\text{liq}}) \quad (26)$$

Figure 26: A screenshot of equations (24a) and (26) from Putirka (2008).

Appendix B

Table 7: Raw chemical analyses of melt inclusions. Blue samples are plagioclase hosted and green samples are olivine hosted.

Samples	SiO ₂	TiO ₂	Al ₂ O ₃	FeO	MnO	MgO	CaO	Na ₂ O	K ₂ O	P ₂ O ₅	Total	Mg#
plag1 incl1	42.93	5.22	7.11	20.43	0.04	10.49	11.42	1.64	0.43	0.30	100.01	47.80
incl plag3	37.94	7.22	5.06	21.54	0.04	6.02	17.26	1.26	0.52	3.14	100.00	33.3
mi1	37.49	9.95	6.44	20.96	0.58	7.10	12.59	2.66	0.56	1.67	100.00	37.7
mi2	47.05	5.94	17.01	8.76	0.27	3.54	12.77	3.51	0.62	0.53	100.00	41.9
plag2 incl	43.13	5.18	12.87	18.29	0.04	6.71	10.04	3.11	0.55	0.07	99.99	39.5
incl3 plag4	41.67	5.64	5.86	22.13	0.04	11.79	11.37	1.05	0.31	0.14	100.00	48.7
incl2 plag4	43.43	5.22	8.33	17.71	0.52	10.49	10.86	2.58	0.57	0.28	99.99	51.4
mi3	50.39	2.96	15.04	7.14	0.04	9.78	9.96	3.96	0.62	0.11	100.00	70.9
incl olivine4	48.45	2.61	17.60	7.12	0.04	6.31	14.04	2.19	1.60	0.04	100.00	61.2
incl olivine6	47.61	2.83	13.84	10.37	0.04	12.70	8.70	3.27	0.62	0.04	100.02	68.6
incl1 ol4	49.83	2.01	15.27	8.92	0.04	10.19	8.73	3.10	1.78	0.12	99.99	67.1
incl2 ol4	51.51	4.39	16.21	4.98	0.04	3.07	15.27	2.56	1.04	0.93	100.00	52.4

Appendix C

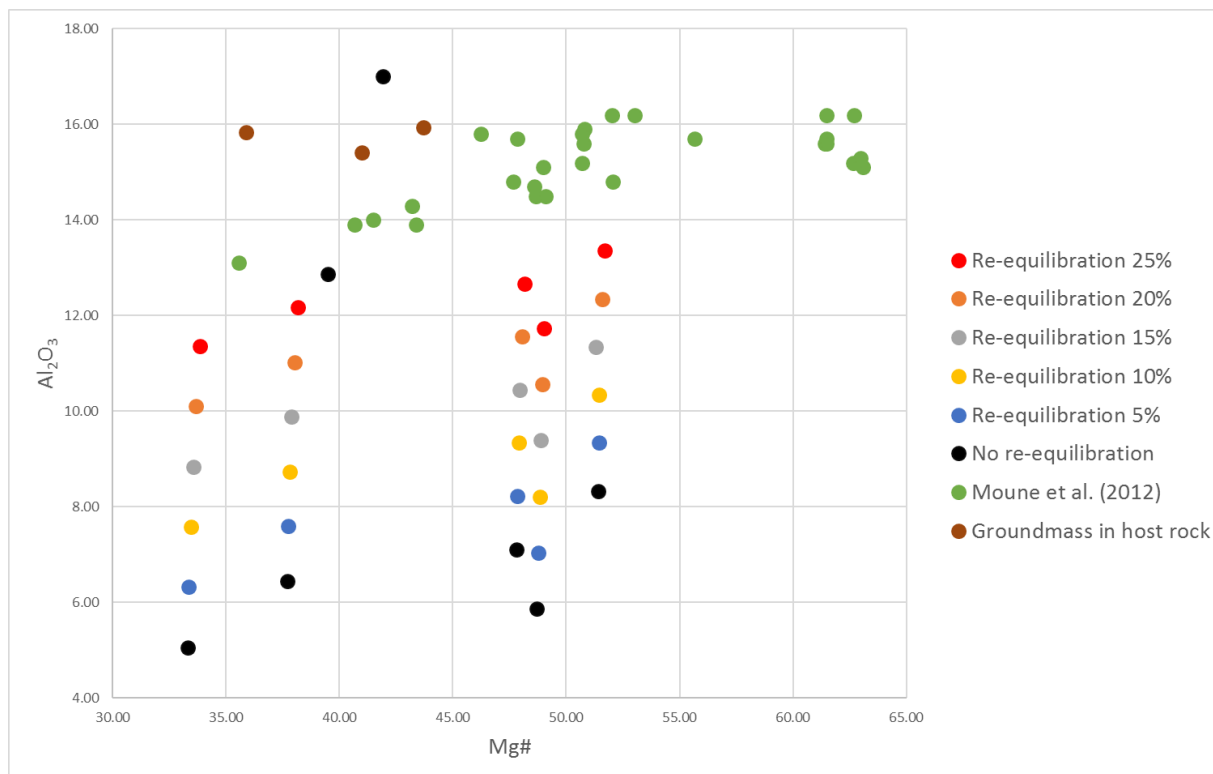


Figure 27: Graph showing the trend of re-equilibration from 0-25%, with melt inclusions compositions from Moune et al. (2012) and groundmass in host rock from Kristjánsson (2015).

Appendix D

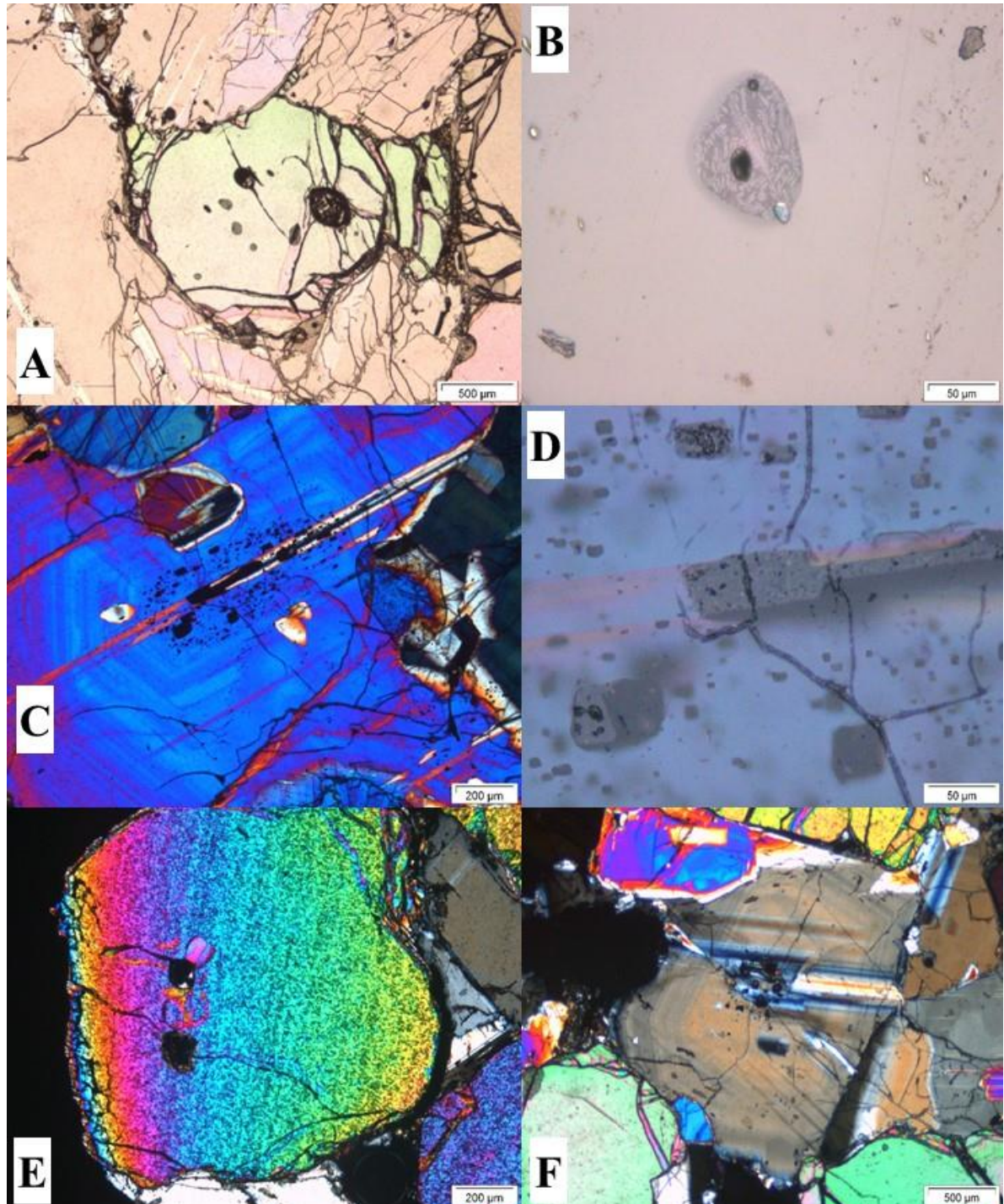


Figure 28: Pictures from the polarization microscope of olivine, plagioclase and melt inclusions. A shows olivine with several melt inclusions. B is a melt inclusion in reflective light. C a zoned plagioclase with many melt inclusions in the core. D close-up of a melt inclusion in the plagioclase from C by reflected light. E a zoned olivine at the contact with the host rock. F zoned plagioclase.

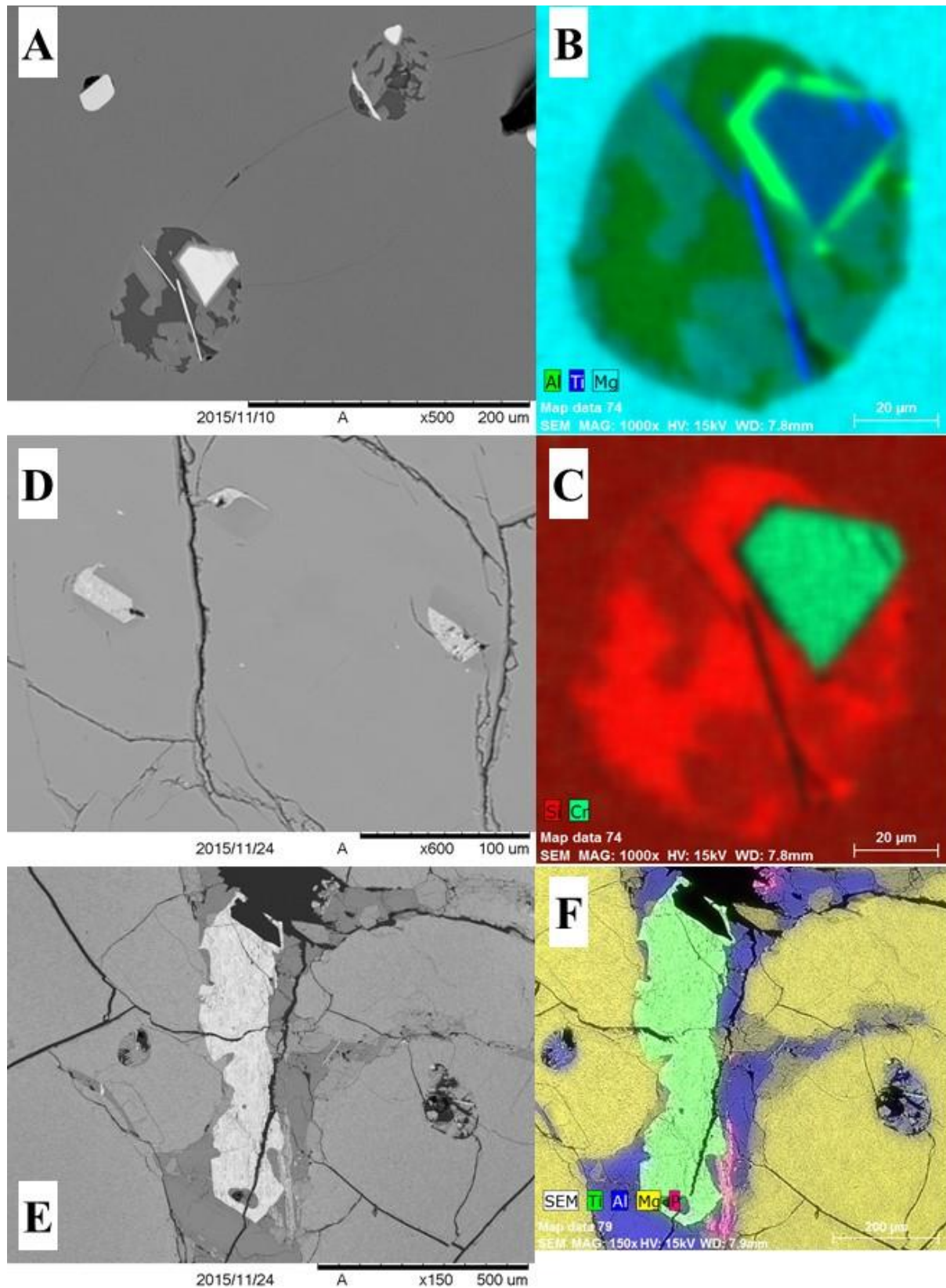


Figure 29: SEM pictures of the troctolite. A shows two melt inclusion in olivine along with spinel. B and C chemical maps of a melt inclusion and a spinel from A. D shows three melt inclusions in plagioclase. E showing olivine, oxide, pyroxene and melt inclusions, note the dark haloes around them indicating extensive PEC. F chemical map of the same are as in E, here one can observe a rather large phosphorus rich crack in the bottom of the photo.